BRIEF COMMUNICATION

Endogenous ZAP affects Zika virus RNA interactome

Ahmad Jawad Sabir[1,a], Nguyen Phuong Khanh Le[2,a], Prince Pal Singh[2,3,a], Uladzimir Karniychuk[2,*]

[1]Department of Microbiology and Immunology, University of Illinois, College of Medicine, Chicago, IL, USA

[2]Department of Veterinary Biosciences, College of Veterinary Medicine, The Ohio State University, Columbus, OH, USA

[3]School of Public Health, University of Saskatchewan, Saskatoon, Canada

[a]**:** These authors contributed equally

*** Correspondence:** Uladzimir Karniychuk
Department of Veterinary Biosciences, College of Veterinary Medicine, The Ohio State University, Columbus, OH, USA
karniychuk.1@osu.edu

Abstract

One of the most recent advances in the analysis of viral RNA–cellular protein interactions is the Comprehensive Identification of RNA-binding Proteins by Mass Spectrometry (ChIRP-MS). Here, we used ChIRP-MS in mock-infected and Zika-infected wild-type cells and cells knockout for the zinc finger CCCH-type antiviral protein 1 (ZAP). We characterized "ZAP-independent" and "ZAP-dependent" cellular protein interactomes associated with flavivirus RNA and found that ZAP affects cellular proteins associated with Zika virus RNA. The ZAP-dependent interactome identified with ChIRP-MS provides potential ZAP co-factors for antiviral activity against Zika virus and possibly other viruses. Identifying the full spectrum of ZAP co-factors and mechanisms of how they act will be critical to understanding the ZAP antiviral system and may contribute to the development of antivirals.

Keywords: Flavivirus, Zika virus, Japanese encephalitis virus, West Nile virus, Zinc finger antiviral protein, ZAP, RNA, RNA helicase, interactome

INTRODUCTION

Emerging flaviviruses constantly threaten public health. The National Institute of Allergy and Infectious Diseases classifies flaviviruses—Zika virus, Japanese encephalitis virus (JEV), yellow fever virus (YFV), and West Nile virus (WNV) as a "Category B Priority," the 2nd highest priority of emerging pathogens and biodefense threats. Zika virus caused the human epidemic in 2015 and persists in at least 89 countries. Japanese encephalitis virus causes encephalitis in humans in the Asia-Pacific region [1], with 68,000 annual cases and 15,000 deaths [2]. There is a concern that JEV can be introduced into North America given the large population of amplifying hosts—pigs and wild boars, and susceptible *Culex* mosquitoes [3-5]. Japanese encephalitis virus keeps expanding—the 2022 JEV outbreak in Australia with infections in swine herds, zoonotic transmission, and human deaths was caused by genotype IV which was not associated with outbreaks before [6]. West Nile virus is the most common arthropod-borne virus in the US. In 2022, the US Centers for Disease Control and Prevention reported 1,126 cases and 93 deaths. In 2023, there were 2,406 human cases in the US, including 1,599 neuroinvasive diseases. The rising number of human cases caused by mosquito-borne flaviviruses shows the lack or inefficiency of environmental controls. There are no approved human vaccines for some flaviviruses (i.e., Zika, WNV). Also, there are no licensed antivirals against flaviviruses because of a knowledge gap in cellular pathways controlling infections, including the knowledge gap in interactions of viral RNA with cellular proteins.

High-throughput methods enable global analysis of viral RNA–cellular protein interactions. One of the most recent advances in analysis of viral RNA–cellular protein interactions is the Comprehensive Identification of RNA-binding Proteins by Mass Spectrometry (ChIRP-MS) [7],

70 where interactions between cellular proteins and genomic RNA of several viruses were profiled
71 that advanced the fundamental knowledge of RNA viruses and informed novel antivirals [8-11].
72 To our knowledge, all these ChIRP-MS studies were done in wild-type cell lines. And comparative
73 ChIRP-MS studies on viral RNA–cellular protein interactions in wild-type and knockout (KO) cell
74 lines are not reported.
75
76 The zinc finger CCCH-type antiviral protein 1, also known as ZAP, ZC3HAV1, or PARP13, is a
77 cellular protein with broad antiviral activity. The protein was first characterized to inhibit murine
78 leukemia virus [12] and later alphaviruses, filoviruses, influenza virus, porcine reproductive and
79 respiratory syndrome virus, hepatitis B virus, human cytomegalovirus, human T cell leukaemia
80 virus type 1, and human immunodeficiency virus-1 [13-23]. The previous study in A549 cells
81 showed JEV sensitivity to ectopic and endogenous ZAP [24]. In the same study, Zika virus was
82 not sensitive to ectopic ZAP; the sensitivity of Zika virus to endogenous ZAP was not tested [24].
83 Another study using ZAP wild-type and ZAP knockout A549 cells showed that wild-type Zika
84 virus was also not sensitive to antiviral ZAP effects [25]. However, our recent study revealed that
85 Zika virus was sensitive to endogenous ZAP in VERO cells. Specifically, we observed reduced
86 viral RNA, infectious titers, and Zika virus NS5 protein expression in wild-type cells compared to
87 ZAP knockout cells [26]. This discrepancy may be due to the different cell lines used: previous
88 studies utilized A549 cells derived from human lung cancer tissue [24], while we used VERO cells
89 from a healthy monkey. Antiviral signaling for many cellular proteins can be highly cell-specific
90 [27]. Another factor is the species difference: the previous study used a human cell line, and we
91 used an African green monkey cell line, a possible natural reservoir host of Zika virus [28].

92 Species-specific ZAP effects are documented [29,30], but comparative studies on ZAP antiviral
93 activity between primates are lacking.
94
95 ZAP binds viral RNA and evokes antiviral activity by mediating viral RNA degradation and
96 translational inhibition [31]. It also interacts with various cellular proteins that may act as co-
97 factors, enhancing its antiviral effects [32]. Furthermore, ZAP can augment other antiviral systems
98 [14,26]. To better understand ZAP–viral RNA–cellular protein interactions, here we used Zika
99 virus infection in wild-type and ZAP knockout VERO cells as a model. Specifically, we used
100 ChIRP-MS in mock-infected and Zika-infected wild-type and ZAP knockout cells to characterize
101 "ZAP-independent" and "ZAP-dependent" cellular protein interactomes associated with flavivirus
102 RNA. Our findings suggest that ZAP influences cellular proteins associated with Zika virus RNA.
103

104 **RESULTS**

105 **Endogenous ZAP affects flavivirus infection phenotypes in VERO cells**

106 While Zika virus was designated as ZAP-resistant in A549 cells [24,25], in our recent study, we
107 showed that Zika virus is sensitive to endogenous ZAP in VERO cells with reduced levels of viral
108 RNA, infectious titers, and NS5 protein expression [26]. Previously we used the multiplicity of
109 infection (MOI) of 1 for comparative studies in VERO wild-type (VERO-ZAP-WT) and knock-
110 out (VERO-ZAP-KO) cell lines [26]. Here to further confirm antiviral ZAP effects against Zika
111 virus we conducted comparative studies in the same cells with low MOI 0.01. We also included
112 into the comparative study JEV previously shown to be sensitive to endogenous and ectopically
113 overexpressed ZAP, and WNV with unknown sensitivity to ZAP in VERO cells.
114

115 For all flaviviruses, we observed a significant ($p < 0.0001$) reduction in E protein expression in
116 VERO-ZAP-WT compared to VERO-ZAP-KO cells (**Figs 1A**, **B**, **E**, **F**, **I**, **J**, and **Figs S1, S2, S3**).
117 All three flaviviruses also showed a considerable reduction of NS5 protein expression in VERO-
118 ZAP-WT compared to VERO-ZAP-KO cells (**Figs 1D**, **H**, **L**). West Nile virus showed comparable
119 intracellular viral RNA loads (p = 0.1875) in both VERO-ZAP-WT and VERO-ZAP-KO cells
120 (**Fig 1K**). Consistent with the reduction of E and NS5 protein expression, Zika virus and JEV had
121 significantly higher intracellular RNA loads in VERO-ZAP-KO cells than in VERO-ZAP-WT
122 cells (p = 0.0012 and 0.0007; **Figs 1C, G**).
123
124 Altogether, we confirmed ZAP antiviral effects against JEV and Zika virus, and demonstrated, for
125 the first time to our knowledge, the sensitivity of WNV to ZAP in VERO cells. Different infection
126 phenotypes in VERO-ZAP-KO than in VERO-ZAP-WT cells suggested ZAP effects mediated via
127 viral RNA binding activity which may involve interactions with other cellular proteins. This
128 motivated us to conduct a ChIRP-MS study to characterize "ZAP-independent" and "ZAP-
129 dependent" cellular protein interactomes associated with Zika virus RNA.
130
131 **ChIRP-MS uncovers ZAP-dependent Zika virus RNA interactome**
132 To define the ZAP-depended host protein interactome associated with Zika genomic RNA, we
133 used the RNA-directed proteomic discovery method ChIRP-MS [7-11] in VERO-ZAP-WT and
134 VERO-ZAP-KO cell lines. We crosslinked mock-infected and virus-infected cell lines with
135 formaldehyde to preserve viral RNA–protein complexes and applied biotinylated oligonucleotides
136 (**Table S1A**) tiling the entire Zika virus RNA to enrich viral RNA–host protein complexes (**Fig**
137 **2A**).

138 For the Zika virus comparative study in VERO-ZAP-WT and VERO-ZAP-KO cells, we used
139 equal MOIs for inoculation to identify ZAP effects on infection phenotypes (**Fig 1**). However, the
140 different infection phenotypes in VERO-ZAP-WT and VERO-ZAP-KO cells (**Fig 1**) pose a
141 challenge for ChIRP-MS study where it is essential to induce equal Zika virus RNA loads in both
142 cell lines for an accurate comparison of ZAP-dependent and ZAP-independent interactomes. Thus,
143 before comparing viral RNA–host protein interactions, we tested different Zika MOIs for
144 inoculation of ZAP-WT and ZAP-KO cells to ensure similar viral RNA loads at the time of
145 formaldehyde fixation and accurate comparative ChIRP-MS. For this, we incrementally increased
146 the MOI for VERO-ZAP-WT cells, as Zika virus caused a more aggressive infection in VERO-
147 ZAP-KO cells (**Fig 1**). The multiplicity of infection 10 for VERO-ZAP-WT cells and MOI 2 for
148 VERO-ZAP-KO cells evoked similar Zika virus loads. To exclude the effects of differential uptake
149 of the stimulus during MOI 10 inoculation of VERO-ZAP-WT cells, during VERO-ZAP-KO MOI
150 2 inoculation we added heat-inactivated Zika virus equivalent of MOI 8. After extensive washing
151 and 72 h incubation, the same Zika antigen loads in VERO-ZAP-WT and VERO-ZAP-KO cells
152 were confirmed with viral E protein staining (**Fig 2B**). The same Zika RNA loads in VERO-ZAP-
153 WT and VERO-ZAP-KO cells were also confirmed using Zika-specific RT-qPCR and next-
154 generation-sequencing (NGS) in sonicated cellular lysates (**input**) and immunoprecipitated viral
155 RNA-protein complexes (**enriched**) (**Figs 2C, D; Fig S4; Supplemental Dataset 1**). High RT-
156 qPCR Zika loads and nearly entire Zika genomic coverage with high NGS depth (**Figs 2C, D; Fig**
157 **S4**) confirms that the ChIRP method efficiently recovered the same high loads of viral RNA in
158 both VERO-ZAP-WT and VERO-ZAP-KO cells. Also, as expected, viral RNA loads were
159 consistently and considerably (around 10^1 difference) higher in enriched than in input samples in
160 RT-qPCR and NGS assays (**Figs 2C, D; Fig S4**). Altogether, we confirmed normalized viral loads

161 and comparable enrichment of viral RNA during ChIRP in VERO-ZAP-WT and VERO-ZAP-KO
162 cells, permitting quantitative comparison of proteins associated with viral RNA between wild-type
163 and ZAP-KO cells.
164
165 Next, we used the Mass Spectrometry Interaction STatistics (MiST) to analyze raw ChIRP-MS
166 data (**Supplemental Dataset 2**) previously applied in ChIRP-MS studies [11,33,34]. We employed
167 MiST with default parameters and used the Singleton Filtering option to exclude proteins with
168 spectral counts in only one biological replicate, quantifying proteins with a MiST score of 0.75 or
169 above [11,33,34]. Additionally, we excluded proteins that had at least one spectral count in any
170 biological replicate of mock-infected wild-type or ZAP-KO cells [11,32]. We applied three
171 analytical strategies to analyze ChIRP-MS data (**Table S1**):
172
173 For the first analytical strategy, using the raw ChIRP-MS data with a total of 2,269 proteins (**Table**
174 **S1B**), we identified proteins specifically associated with Zika virus RNA in VERO-ZAP-WT cells.
175 We defined the resultant list of enriched proteins as the "extended" Zika virus RNA interactome
176 in VERO-ZAP-WT cells. This extended interactome contains 383 proteins (**Table S1C**). We
177 named this interactome "extended" because additional control criteria were applied to narrow
178 down and enrich the "ZAP-dependent" Zika virus RNA interactome (see below).
179
180 ChIRP-MS is a rather new technique in molecular biology; the first time it was described for
181 systemic identification of cellular proteins interacting with cellular mRNA in 2015 [7]. From 2019,
182 several virology groups have applied ChIRP-MS to characterize interactions between cellular
183 proteins and genomic RNA of severe acute respiratory syndrome coronavirus 2, Ebola virus,

184 dengue virus, and Zika virus in wild-type ZAP-positive cells [8-11]. Thus, we compared our
185 extended Zika virus RNA interactome in VERO-ZAP-WT cells with the Zika interactome in Huh
186 cells from a previous publication [10]. A similar number of proteins was reported here—383, and
187 previously—395. The comparison also showed a good reproducibility of 25.4 % between two
188 protein sets (**Table S1D**). We consider 25.4% a good reproducibility because studies were done in
189 cells of different species—nonhuman primates (VERO) and humans (Huh), with different MOIs
190 and sampling time points.
191 The specificity of our ChIRP-MS is also confirmed by physical associations between Zika virus
192 RNA and viral prM, C, E, NS1, NS2A, NS2B, NS3, and NS5 proteins in only infected cells, while
193 all mock-infected replicates were negative (**Table S1E**). The enrichment of viral proteins provides
194 evidence that ChIRP-MS covers interactions across the entire length of viral RNA [8]. Analysis of
195 the MiST abundance score and absolute spectral counts showed that the viral NS3 and NS5
196 proteins were most strongly recovered (**Table S1E**; NS3 MiST abundance score 0.167, NS5 MiST
197 abundance score 0.304; NS3 mean spectral counts 39, NS5 mean spectral counts 102), which is
198 consistent with previous ChIRP-MS Zika virus study where NS3 and NS5 were also most abundant
199 [10]; and with direct binding function of flavivirus NS3—RNA helicase, and NS5—RNA-
200 dependent RNA polymerase.
201
202 Analyzes of top interacting cellular proteins with the highest spectral counts and GO enrichment
203 analysis also suggested the specificity of ChIRP-MS. All top 15 interacting proteins (except
204 NCOA5) with the highest spectral counts (**Fig 3A**) are known factors of RNA biology, including
205 RNA binding, RNA splicing, and RNA helicase activities (**Table S1C**). Gene Ontology

206 enrichment analysis also showed that all seven enriched pathways with at least two-fold
207 enrichment represent nucleic acid/RNA binding and RNA biology processes (**Fig 3D**).
208 For the second analytical strategy, we identified proteins specifically interacting with Zika virus
209 RNA in VERO-ZAP-KO cells. For specificity, we applied the same strategy as above: We selected
210 the Singleton Filtering MiST option to exclude proteins with spectral counts in only one biological
211 replicate and quantify proteins with the MiST score of 0.75 or above [11,33,34]. We also excluded
212 all proteins with a single spectral count in at least one of three biological replicates in mock-
213 infected wild-type or ZAP-KO cells. We defined the resultant list of enriched proteins as a "ZAP-
214 independent" Zika virus RNA interactome. We defined this interactome as ZAP-independent
215 because associated cellular proteins were discovered in VERO-ZAP-KO cells showing the ZAP-
216 independent nature of interactions. The ZAP-independent interactome contains 116 proteins
217 (**Table S1F**). As expected, most, 13 out of 15 top cellular interacting proteins with the highest
218 spectral counts are known factors in RNA biology (**Fig 3B**; **Table S1F**). Zika virus proteins were
219 identified in only infected VERO-ZAP-KO cells (**Table S1G**).
220
221 Finally, to discover the "ZAP-dependent" Zika RNA interactome in VERO-ZAP-WT cells, in
222 addition to the above specificity exclusion criteria in MiST settings and mock-infected cells, we
223 excluded proteins that had at least one spectral count in at least one of the three biological replicates
224 in VERO-ZAP-KO cells infected with Zika virus. The ZAP-dependent interactome contains 209
225 proteins (**Table S1H**). The ZAP-dependent Zika RNA interactome has more proteins than ZAP-
226 independent—209 versus 116 proteins. The difference in 93 proteins between interactomes in
227 ZAP-WT and ZAP-KO cells is rational because in the previous study a tandem mass spectrometry
228 showed that 114 cellular proteins interact with the overexpressed immunoprecipitated ZAP large

229 isoform in uninfected cells [32]. Other large-scale interactome studies in uninfected cells have
230 identified more than 250 potential cellular proteins that may potentially interact with ZAP [32,35-
231 38].
232
233 As expected, most, 12 out of 15 top interacting proteins with the highest spectral counts in the
234 ZAP-dependent interactome are known factors in RNA biology (**Fig 3C**; **Table S1H**).
235 Comparative GO enrichment analysis between ZAP-independent and ZAP-dependent
236 interactomes showed only one enriched pathway related to RNA biology in ZAP-KO cells and six
237 enriched RNA biology pathways in ZAP-WT cells, including "helicase activity" with the highest
238 fold enrichment (**Figs 3E, F**). Accordingly, among the top 15 proteins in the ZAP-dependent
239 interactome four proteins were RNA helicases (**Table S1H**). In total, 11 RNA helicases were
240 enriched in the ZAP-dependent interactome—DDX42, DDX56, DDX27, DDX50, DDX52,
241 DDX23, DDX54, DDX18, DHX57, DDX47, and one uncharacterized RNA helicase (**Tables S1H,**
242 **I**).
243
244 Altogether, using ChIRP-MS and MiST analysis, we characterized the cellular interactome
245 associated with Zika virus RNA, including Extended, ZAP-independent, and ZAP-dependent
246 interactomes.
247
248 **ZAP wild-type and knockout VERO cells express DDX RNA helicases**
249 ZAP binds cellular mRNA and affects gene expression, including antiviral and immune resolution
250 transcriptional responses [39,40]. Thus, it was unclear whether the enrichment of RNA helicases
251 in the ChIRP ZAP-dependent Zika interactome (**Tables S1H; Figs 3C, F**) and the depletion of

252 RNA helicases in the ChIRP ZAP-independent Zika interactome (**Tables S1F; Figs 3B, E**) were
253 exclusively due to direct ZAP–viral RNA–cellular RNA helicase interactions in ZAP-WT cells
254 and the lack of such interactions in ZAP-KO cells, or ZAP-mediated effects on cellular RNA
255 helicase mRNAs also played a role. Therefore, we quantified the protein levels of four selected
256 helicases (DDX23, DDX27, DDX42, and DDX50) using Western blot in MOCK and infected
257 ZAP-WT and ZAP-KO cells (the same MOI and sampling time as for the ChIRP-MS experiment).
258 DDX42 and DDX27 were chosen because they were among the top three enriched helicases (**Table**
259 **S1I**). DDX23 and DDX50 are known to have antiviral activity [41,42].
260
261 Western blot analysis revealed expression of all four RNA helicases in both VERO-ZAP-KO and
262 VERO-ZAP-WT cells, under mock condition and during Zika virus infection (**Fig 4A**). The
263 expression of DDX23 and DDX27 was lower in both MOCK and Zika virus-infected ZAP-KO
264 cells compared to ZAP-WT cells (DDX23 $p = 0.0374$; $p = 0.0471$; DDX27 $p < 0.0001$; $p = 0.0004$),
265 although ZAP-KO cells still showed prominent DDX23 and DDX27 expression (**Figs 4A, B**). Zika
266 virus infection significantly reduced DDX27 expression in both cell lines (ZAP-KO $p=0.415$;
267 ZAP-WT $p=0.001$) (**Fig 4A, B**). The expression of DDX42 was significantly lower in mock-
268 infected ZAP-WT than in ZAP-KO cells ($p = 0.0179$). Zika virus infection considerably reduced
269 DDX42 expression in both cell lines, but the comparative expression in ZAP-KO and ZAP-WT
270 cells during infection was similar ($p = 0.2139$) (**Figs 4A, B**). The expression of DDX50 was lower
271 in both MOCK and Zika virus-infected ZAP-KO cells compared to ZAP-WT cells (MOCK $p =$
272 0.0001; Zika $p < 0.0001$), although ZAP-KO cells still showed prominent DDX50 expression (**Figs**
273 **4A, B**). Zika virus infection did not affect DDX50 expression in either cell line (**Fig 4A, B**).
274

275 Overall, we confirmed that ZAP-WT and ZAP-KO cells express all four tested RNA helicases—
276 DDX23, DDX27, DDX42, and DDX50. However, ZAP knockout was associated with reduced
277 DDX23, DDX27, and DDX50 expression in both MOCK and infection conditions. These reduced
278 cellular expressions of DDX23, DDX27, and DDX50 suggest that ZAP-mediated effects on
279 cellular RNA helicase mRNAs may contribute to the depletion of RNA helicases in the ChIRP
280 ZAP-independent Zika interactome. In contrast, DDX42 expression was even in ZAP-KO and
281 ZAP-WT cells during Zika virus infection, indicating that direct interactions between ZAP, viral
282 RNA, and cellular RNA helicases in ZAP-WT cells may play the central role in the enrichment of
283 RNA helicases in the ChIRP ZAP-dependent Zika interactome.
284
285 **DISCUSSION**
286 All previous ChIRP-MS studies on a viral RNA-cellular protein interactome were done in wild-
287 type cell lines [8-11], and comparative ChIRP-MS studies in wild-type and KO cells were not
288 reported. Here, using ChIRP-MS in ZAP-WT and ZAP-KO cells, we delineated ZAP-independent
289 and ZAP-dependent cellular protein interactomes associated with Zika virus RNA. We showed
290 that such experimental approach is feasible by normalizing MOIs and viral loads in ZAP-WT and
291 ZAP-KO cells. Despite extensive research on ZAP's antiviral activity, to our knowledge, this study
292 is the first to explore the ZAP-dependent interactome specifically associated with viral RNA.
293
294
295 ZAP requires RNA helicases as co-factors: ZAP's N-terminus interacts with the N- and C-terminal
296 domains of DDX17 that promotes ZAP-mediated degradation of murine leukemia reporter virus
297 [43]. However, our ChIRP-MS Zika data do not contain p72 DEAD-box RNA helicase (DDX17)

298 (**Table S1B**). DHX30 interacts with ZAP, and the knockdown of DHX30 reduces ZAP's antiviral
299 activity against murine leukemia reporter virus [44]. Accordingly, we identified DHX30 in ChIRP-
300 MS data (**Table S1B**); however, it was excluded from further interactome-specific analysis with
301 our rigorous specificity cutoff. Interestingly, we found that 11 RNA helicases were enriched in the
302 ZAP-dependent interactome—DDX42, DDX56, DDX27, DDX50, DDX52, DDX23, DDX54,
303 DDX18, DHX57, DDX47, and one uncharacterized RNA helicase. In contrast, in the ZAP-
304 independent interactome, no RNA helicases were enriched. The limitation is that our experimental
305 design does not allow to identify the specific nature of interactions between Zika virus RNA and
306 cellular proteins. We do not know yet which cellular proteins interact with only ZAP bound to
307 viral RNA, which interact with ZAP and viral RNA, and which proteins have strict viral RNA
308 dependency during interactions with ZAP. ZAP binds to single-stranded viral RNA and potentially
309 to single overhangs in double-stranded RNA [45,46]; RNA helicases can bind to double-stranded
310 RNA, single overhangs in double-stranded RNA, and single-stranded RNA; these make
311 interactions between ZAP, viral RNA, and RNA helicases spatially possible. Additional research
312 is necessary to determine if the RNA helicases identified in this study function as co-factors for
313 ZAP in its antiviral activity, specifically ZAP-mediated degradation of viral RNA.

314

315 In addition to RNA helicases, ZAP requires other co-factors. It lacks intrinsic RNase activity but
316 recruits the 5' and 3' RNA degradation machinery [24,47]. The E3 ubiquitin ligase TRIM25 is
317 important for ZAP activity against alphaviruses by increasing inhibition of viral translation
318 [48,49]. ZAP also interacts with the cytoplasmic protein KHNYN to inhibit CpG-enriched HIV-1
319 [50]. Riplet, a protein known to play a central role in activating the retinoic acid-inducible gene I
320 (RIG-I), has been recently identified as a ZAP co-factor that augments the restriction of HIV-1

321 [51]. However, the full complexity of cellular proteins essential for ZAP antiviral activity is
322 unknown. Large-scale interactome studies in non-infected cells have identified more than 250
323 proteins that may interact with ZAP [32,35-38]. Notably, there were no large-scale ZAP
324 interactome studies in the context of viral infection [35]. Thus, our ZAP-dependent ChIRP-MS
325 interactome (**Table S1H**) provides a highly specific list of potential ZAP co-factors, including
326 eleven RNA helicases for future mechanistic and functional studies.
327
328
329 It is known that DDX RNA helicases not only facilitate viral RNA degradation but also act as viral
330 RNA sensing proteins contributing to cellular innate immune signaling, type I IFN production, and
331 antiviral response [52-57]. Also, viruses can abduct cellular RNA helicases to support their
332 lifecycle and promote infectivity [58,59]. Cellular RNA helicases often interact with microbial
333 genomes and evoke their properties in the complex with different adaptor proteins [52-54,56,60-
334 62]. Thus, ZAP may play a dual role in mediating RNA helicase-dependent antiviral and proviral
335 effects. Before our ChIRP-MS study, such co-factor/adaptor role of ZAP in interactions between
336 viral RNA and cellular RNA helicases was not considered.
337
338
339 Interestingly, Western blot analysis showed that ZAP expression is associated with higher levels
340 of at least three RNA helicases—DDX23, DDX27, and DDX50—since their expression was
341 reduced in both MOCK and infected ZAP-KO cells as compared to ZAP-WT cells (**Fig 4**). Thus,
342 ZAP may indirectly contribute to antiviral cellular responses by maintaining the expression of
343 RNA helicases, which are known to have antiviral activity, including DDX23 and DDX50 [41,42].

344 Another interesting finding is that Zika virus infection considerably reduced the expression of
345 DDX23, DDX 27, and DDX42 in ZAP-WT cells (**Fig 4**), as well as ZAP (**Fig S3**) under our
346 experimental conditions (72 h post-infection). These observations may indicate Zika virus
347 strategies for evading cellular immune responses, warranting further investigation.
348
349
350 The primary limitation of this study is its focus on an associative ChIRP-MS comparison between
351 ZAP-WT and ZAP-KO cells. While conducting functional studies could provide further insights,
352 it falls beyond the scope of this work. Nonetheless, our ZAP-dependent interactome offers the
353 scientific community a valuable resource for future studies on ZAP, its co-factors, and viral RNA
354 interactions. It would also be interesting to compare ChIRP-MS interactomes across different
355 ZAP-WT and ZAP-KO cell lines infected with various viruses. Our strict filtering approach to
356 identify the ZAP-dependent interactome, which excluded proteins from the ZAP-independent
357 interactome even with a single MS spectral count in ZAP-KO cells, might be seen as too rigorous.
358 However, it ensures a highly specific list of potential ZAP co-factors. Additionally, we have made
359 available the raw and extended ZAP interactome databases (**Table S1B, C; Supplemental Dataset**
360 **2**), allowing others to apply their own filtering approaches.
361
362 **CONCLUSIONS**
363 Together, the ZAP-dependent interactome identified with ChIRP-MS provides potential ZAP co-
364 factors for antiviral activity against Zika virus and possibly other viruses. Identifying the full
365 spectrum of ZAP co-factors and mechanisms of how they act will be critical to understand the
366 ZAP antiviral system and may contribute to the development of antivirals.

367 **MATERIALS AND METHODS**

368 Details of ChIRP-MS, cells, viruses, comparative infection studies, RT-qPCR, Western blot, and
369 statistics are in Supplemental Materials and Methods.

370

371 **DISCLOSURE STATEMENT**

372 The authors declare that the research was conducted in the absence of any commercial or financial
373 relationships that could be construed as a potential conflict of interest.

374

375 **AUTHOR CONTRIBUTIONS**

376 Conceptualization: UK. Investigation: NPKL, AJS, PPS, UK. Data analysis: NPKL, AJS, PPS,
377 UK. Funding: UK. Resources: UK. Writing—original draft preparation: NPKL, AJS, PPS, UK.
378 Writing—review and editing: UK, NPKL, PPS.

379

380 **FUNDING**

381 PPS received a Scholarship from the School of Public Health, University of Saskatchewan. This
382 work was partially supported by a grant to UK from the Canadian Institutes of Health Research
383 (CIHR; Project Grant #424307). The funders had no role in study design, data collection and
384 analysis, decision to publish, or manuscript preparation.

385

386 **DATA AVAILABILITY**

387 Data available within the article, its supplementary materials, and DRYAD open data publishing
388 platform which can be accessed via links:

389 https://datadryad.org/stash/share/tqLeKFRU68c947MAFplLF9S8xrd_JM8IulT5JFSiEio
390

and

https://datadryad.org/stash/share/GJWy9A9Hofp-9aya9oOLI9RgDsi_qqw6FITwPu4F0Gs

415 **REFERENCES**

416 1. Amicizia D, Zangrillo F, Lai PL, et al. Overview of Japanese encephalitis disease and its
417 prevention. Focus on IC51 vaccine (IXIARO®). Journal of Preventive Medicine and Hygiene2018.
418 p. E99-E107.
419 2. Tarantola A, Goutard F, Newton P, et al. Estimating the burden of Japanese encephalitis virus
420 and other encephalitides in countries of the mekong region. In: Gray DJ, editor. PLoS neglected
421 tropical diseases2014. p. e2533.
422 3. Oliveira ARS, Piaggio J, Cohnstaedt LW, et al. Introduction of the Japanese encephalitis virus
423 (JEV) in the United States – A qualitative risk assessment. Transboundary and Emerging
424 Diseases2019. p. 1558-1574.
425 4. Huang YJS, Harbin JN, Hettenbach SM, et al. Susceptibility of a North American Culex
426 quinquefasciatus to Japanese Encephalitis Virus. Vector borne and zoonotic diseases
427 (Larchmont, N.Y.): Vector Borne Zoonotic Dis; 2015. p. 709-711.
428 5. Faizah AN, Kobayashi D, Matsumura R, et al. Blood meal source identification and RNA virome
429 determination in Japanese encephalitis virus vectors collected in Ishikawa Prefecture, Japan,
430 show distinct avian/mammalian host preference. J Med Entomol. 2023 Apr 7.
431 6. Howard-Jones AR, Pham D, Jeoffreys N, et al. Emerging Genotype IV Japanese Encephalitis Virus
432 Outbreak in New South Wales, Australia. Viruses. 2022 Aug 24;14(9).
433 7. Chu C, Zhang QC, da Rocha ST, et al. Systematic discovery of Xist RNA binding proteins. Cell.
434 2015 Apr 9;161(2):404-16.
435 8. Flynn RA, Belk JA, Qi Y, et al. Discovery and functional interrogation of SARS-CoV-2 RNA-host
436 protein interactions. Cell. 2021 Apr 29;184(9):2394-2411 e16.
437 9. Labeau A, Fery-Simonian L, Lefevre-Utile A, et al. Characterization and functional interrogation
438 of the SARS-CoV-2 RNA interactome. Cell Rep. 2022 Apr 26;39(4):110744.
439 10. Ooi YS, Majzoub K, Flynn RA, et al. An RNA-centric dissection of host complexes controlling
440 flavivirus infection. Nat Microbiol. 2019 Dec;4(12):2369-2382.
441 11. Zhang S, Huang W, Ren L, et al. Comparison of viral RNA-host protein interactomes across
442 pathogenic RNA viruses informs rapid antiviral drug discovery for SARS-CoV-2. Cell Res. 2022
443 Jan;32(1):9-23.
444 12. Gao G, Guo X, Goff SP. Inhibition of retroviral RNA production by ZAP, a CCCH-type zinc finger
445 protein. Science (New York, N.Y.): American Association for the Advancement of Science; 2002.
446 p. 1703-6.
447 13. Bick MJ, Carroll JW, Gao G, et al. Expression of the zinc-finger antiviral protein inhibits alphavirus
448 replication. J Virol. 2003 Nov;77(21):11555-62.
449 14. Nguyen LP, Aldana KS, Yang E, et al. Alphavirus Evasion of Zinc Finger Antiviral Protein (ZAP)
450 Correlates with CpG Suppression in a Specific Viral nsP2 Gene Sequence. Viruses. 2023 Mar
451 24;15(4).
452 15. Liu CH, Zhou L, Chen G, et al. Battle between influenza A virus and a newly identified antiviral
453 activity of the PARP-containing ZAPL protein. Proc Natl Acad Sci U S A. 2015 Nov
454 10;112(45):14048-53.
455 16. Mao R, Nie H, Cai D, et al. Inhibition of hepatitis B virus replication by the host zinc finger
456 antiviral protein. PLoS Pathog. 2013;9(7):e1003494.
457 17. Muller S, Moller P, Bick MJ, et al. Inhibition of filovirus replication by the zinc finger antiviral
458 protein. J Virol. 2007 Mar;81(5):2391-400.
459 18. Tang Q, Wang X, Gao G. The Short Form of the Zinc Finger Antiviral Protein Inhibits Influenza A
460 Virus Protein Expression and Is Antagonized by the Virus-Encoded NS1. J Virol. 2017 Jan
461 15;91(2).

462 19. Zhu Y, Chen G, Lv F, et al. Zinc-finger antiviral protein inhibits HIV-1 infection by selectively
463 targeting multiply spliced viral mRNAs for degradation. Proc Natl Acad Sci U S A. 2011 Sep
464 20;108(38):15834-9.
465 20. Takata MA, Goncalves-Carneiro D, Zang TM, et al. CG dinucleotide suppression enables antiviral
466 defence targeting non-self RNA. Nature. 2017 Oct 5;550(7674):124-127.
467 21. Miyazato P, Matsuo M, Tan BJY, et al. HTLV-1 contains a high CG dinucleotide content and is
468 susceptible to the host antiviral protein ZAP. Retrovirology. 2019 Dec 16;16(1):38.
469 22. Gonzalez-Perez AC, Stempel M, Wyler E, et al. The Zinc Finger Antiviral Protein ZAP Restricts
470 Human Cytomegalovirus and Selectively Binds and Destabilizes Viral UL4/UL5 Transcripts. mBio.
471 2021 May 4;12(3).
472 23. Zhao Y, Song Z, Bai J, et al. ZAP, a CCCH-Type Zinc Finger Protein, Inhibits Porcine Reproductive
473 and Respiratory Syndrome Virus Replication and Interacts with Viral Nsp9. J Virol. 2019 May
474 15;93(10).
475 24. Chiu HP, Chiu H, Yang CF, et al. Inhibition of Japanese encephalitis virus infection by the host
476 zinc-finger antiviral protein. PLoS Pathogens: Public Library of Science; 2018.
477 25. Fros JJ, Visser I, Tang B, et al. The dinucleotide composition of the Zika virus genome is shaped
478 by conflicting evolutionary pressures in mammalian hosts and mosquito vectors. PLoS Biol. 2021
479 Apr;19(4):e3001201.
480 26. Nguyen Phuong Khanh Le PPS, Ahmad Jawad Sabir, Ivan Trus, Uladzimir Karniychuk. Endogenous
481 ZAP is associated with altered global cellular gene expression during Zika virus infection. bioRxiv.
482 2024. https://doi.org/10.1101/2024.05.23.595518
483 27. Pallett MA, Lu Y, Smith GL. DDX50 Is a Viral Restriction Factor That Enhances IRF3 Activation.
484 Viruses. 2022 Feb 3;14(2).
485 28. Buechler CR, Bailey AL, Weiler AM, et al. Seroprevalence of Zika Virus in Wild African Green
486 Monkeys and Baboons. mSphere. 2017 Mar-Apr;2(2).
487 29. Kerns JA, Emerman M, Malik HS. Positive selection and increased antiviral activity associated
488 with the PARP-containing isoform of human zinc-finger antiviral protein. PLoS Genet. 2008
489 Jan;4(1):e21.
490 30. Goncalves-Carneiro D, Takata MA, Ong H, et al. Origin and evolution of the zinc finger antiviral
491 protein. PLoS Pathog. 2021 Apr;17(4):e1009545.
492 31. Li MMH, Aguilar EG, Michailidis E, et al. Characterization of Novel Splice Variants of Zinc Finger
493 Antiviral Protein (ZAP). J Virol. 2019 Sep 15;93(18).
494 32. Goodier JL, Pereira GC, Cheung LE, et al. The Broad-Spectrum Antiviral Protein ZAP Restricts
495 Human Retrotransposition. PLOS Genetics: Public Library of Science; 2015. p. e1005252.
496 33. Verschueren E, Von Dollen J, Cimermancic P, et al. Scoring Large-Scale Affinity Purification Mass
497 Spectrometry Datasets with MiST. Curr Protoc Bioinformatics. 2015 Mar 9;49:8 19 1-8 19 16.
498 34. Jager S, Cimermancic P, Gulbahce N, et al. Global landscape of HIV-human protein complexes.
499 Nature. 2011 Dec 21;481(7381):365-70.
500 35. Ficarelli M, Neil SJD, Swanson CM. Targeted Restriction of Viral Gene Expression and Replication
501 by the ZAP Antiviral System. Annu Rev Virol. 2021 Sep 29;8(1):265-283.
502 36. Caudron-Herger M, Rusin SF, Adamo ME, et al. R-DeeP: Proteome-wide and Quantitative
503 Identification of RNA-Dependent Proteins by Density Gradient Ultracentrifugation. Mol Cell.
504 2019 Jul 11;75(1):184-199 e10.
505 37. Huttlin EL, Bruckner RJ, Paulo JA, et al. Architecture of the human interactome defines protein
506 communities and disease networks. Nature. 2017 May 25;545(7655):505-509.
507 38. Youn JY, Dunham WH, Hong SJ, et al. High-Density Proximity Mapping Reveals the Subcellular
508 Organization of mRNA-Associated Granules and Bodies. Mol Cell. 2018 Feb 1;69(3):517-532 e11.

509 39. Todorova T, Bock FJ, Chang P. PARP13 regulates cellular mRNA post-transcriptionally and
510 functions as a pro-apoptotic factor by destabilizing TRAILR4 transcript. Nat Commun. 2014 Nov
511 10;5:5362.
512 40. Schwerk J, Soveg FW, Ryan AP, et al. RNA-binding protein isoforms ZAP-S and ZAP-L have distinct
513 antiviral and immune resolution functions. Nat Immunol. 2019 Dec;20(12):1610-1620.
514 41. Abdullah SW, Han S, Wu J, et al. The DDX23 Negatively Regulates Translation and Replication of
515 Foot-and-Mouth Disease Virus and Is Degraded by 3C Proteinase. Viruses. 2020 Nov 25;12(12).
516 42. Han P, Ye W, Lv X, et al. DDX50 inhibits the replication of dengue virus 2 by upregulating IFN-
517 beta production. Arch Virol. 2017 Jun;162(6):1487-1494.
518 43. Chen G, Guo X, Lv F, et al. p72 DEAD box RNA helicase is required for optimal function of the
519 zinc-finger antiviral protein. Proc Natl Acad Sci U S A. 2008 Mar 18;105(11):4352-7.
520 44. Ye P, Liu S, Zhu Y, et al. DEXH-Box protein DHX30 is required for optimal function of the zinc-
521 finger antiviral protein. Protein Cell. 2010 Oct;1(10):956-64.
522 45. Xu S, Ci Y, Wang L, et al. Zika virus NS3 is a canonical RNA helicase stimulated by NS5 RNA
523 polymerase. Nucleic Acids Res. 2019 Sep 19;47(16):8693-8707.
524 46. Luo X, Wang X, Gao Y, et al. Molecular Mechanism of RNA Recognition by Zinc-Finger Antiviral
525 Protein. Cell Rep. 2020 Jan 7;30(1):46-52 e4.
526 47. Zhu Y, Gao G. ZAP-mediated mRNA degradation. RNA Biol. 2008 Apr-Jun;5(2):65-7.
527 48. Li MM, Lau Z, Cheung P, et al. TRIM25 Enhances the Antiviral Action of Zinc-Finger Antiviral
528 Protein (ZAP). PLoS Pathog. 2017 Jan;13(1):e1006145.
529 49. Zheng X, Wang X, Tu F, et al. TRIM25 Is Required for the Antiviral Activity of Zinc Finger Antiviral
530 Protein. Journal of virology: J Virol; 2017.
531 50. Ficarelli M, Wilson H, Pedro Galão R, et al. KHNYN is essential for the zinc finger antiviral protein
532 (ZAP) to restrict HIV-1 containing clustered CpG dinucleotides. eLife2019.
533 51. Buckmaster MV, Goff SP. Riplet Binds the Zinc Finger Antiviral Protein (ZAP) and Augments ZAP-
534 Mediated Restriction of HIV-1. Journal of Virology: American Society for Microbiology; 2022.
535 52. Zhang Z, Kim T, Bao M, et al. DDX1, DDX21, and DHX36 helicases form a complex with the
536 adaptor molecule TRIF to sense dsRNA in dendritic cells. Immunity. 2011 Jun 24;34(6):866-78.
537 53. Kim T, Pazhoor S, Bao M, et al. Aspartate-glutamate-alanine-histidine box motif (DEAH)/RNA
538 helicase A helicases sense microbial DNA in human plasmacytoid dendritic cells. Proc Natl Acad
539 Sci U S A. 2010 Aug 24;107(34):15181-6.
540 54. Zhang Z, Yuan B, Lu N, et al. DHX9 pairs with IPS-1 to sense double-stranded RNA in myeloid
541 dendritic cells. J Immunol. 2011 Nov 1;187(9):4501-8.
542 55. Pattabhi S, Knoll ML, Gale M, Jr., et al. DHX15 Is a Coreceptor for RLR Signaling That Promotes
543 Antiviral Defense Against RNA Virus Infection. J Interferon Cytokine Res. 2019 Jun;39(6):331-
544 346.
545 56. Miyashita M, Oshiumi H, Matsumoto M, et al. DDX60, a DEXD/H box helicase, is a novel antiviral
546 factor promoting RIG-I-like receptor-mediated signaling. Mol Cell Biol. 2011 Sep;31(18):3802-19.
547 57. Ermler ME, Yerukhim E, Schriewer J, et al. RNA helicase signaling is critical for type i interferon
548 production and protection against Rift Valley fever virus during mucosal challenge. J Virol. 2013
549 May;87(9):4846-60.
550 58. Steimer L, Klostermeier D. RNA helicases in infection and disease. RNA Biol. 2012 Jun;9(6):751-
551 71.
552 59. Wu CY, Nagy PD. Role reversal of functional identity in host factors: Dissecting features affecting
553 pro-viral versus antiviral functions of cellular DEAD-box helicases in tombusvirus replication.
554 PLoS Pathog. 2020 Oct;16(10):e1008990.
555 60. Cheng W, Chen G, Jia H, et al. DDX5 RNA Helicases: Emerging Roles in Viral Infection. Int J Mol
556 Sci. 2018 Apr 9;19(4).

557 61. Mitoma H, Hanabuchi S, Kim T, et al. The DHX33 RNA helicase senses cytosolic RNA and
558 activates the NLRP3 inflammasome. Immunity. 2013 Jul 25;39(1):123-35.
559 62. Zhang Z, Yuan B, Bao M, et al. The helicase DDX41 senses intracellular DNA mediated by the
560 adaptor STING in dendritic cells. Nat Immunol. 2011 Sep 4;12(10):959-65.

561
562
563
564
565
566
567
568
569
570
571
572
573
574
575
576
577
578
579
580
581
582
583
584
585
586
587

588 **FIGURE LEGENDS**

589 **Fig 1. ZAP affects JEV, Zika, and WNV infection phenotypes.** Representative images of cells
590 positive for JEV (**A**), Zika virus (**E**), and WNV (**I**) E protein (red staining) at 72 h (48 h for WNV),
591 MOI 0.01. Magnification x200. The experiment was done in 3 biological and 3 technical replicates.
592 Figures represent the general patterns in all replicates. All 9 replicates for VERO-ZAP-WT and
593 VERO-ZAP-KO cells are shown in **Fig S1**. The digital quantification of JEV (**B**), Zika (**F**), and
594 WNV (**J**) positive cells in all 9 replicates from **Fig S1**. *****Unpaired t-test: $P < 0.05$. In mock-infected
595 cells digital sensitive counting represents the staining background. The fold increase of JEV (**C**),
596 Zika (**G**), and WNV (**K**) RNA loads in cell lysates collected at 1 h and 72 h (48 h for WNV) after
597 inoculation. VERO-WT and VERO-ZAP-KO cells were inoculated with MOI 0.01. Virus
598 inoculums were removed and replaced with media. Cell lysates were collected with a lysis buffer
599 at 1 h post-inoculation (to normalize for leftover virus inoculum RNA) and at 48-72 h. *****Unpaired
600 t-test: $P < 0.05$. The experiment was done in 3 biological and 2 technical replicates. (**D**, **H**, **L**)
601 Reduced flavivirus infection in VERO-ZAP-WT cells at 72 h (48 h for WNV) represented by
602 western blot for NS5 proteins. Normalized 50 µg of protein was used for all samples. Two
603 biological replicates for each condition are shown.
604
605 **Fig 2. ChIRP-MS study design and validation. (A)** ChIRP-MS experimental design to compare
606 viral RNA–host protein interactions in ZAP-positive and ZAP-KO cells. ChIRP-MS was done in
607 three biological replicates; each biological replicate consisted of lysed cells from four T-175 flasks
608 for each experimental condition. **(B)** We adapted normalized MOIs to induce similar Zika viral
609 loads in ZAP-WT and ZAP-KO cells. Red staining represents a similar number of Zika virus E
610 protein-positive cells in WT and KO cells. Inserts—mock-infected cells. **(C)** The same Zika RNA
611 loads in ZAP-WT and ZAP-KO cells were also confirmed using RT-qPCR. **Input** - sonicated
612 cellular lysates. **Enriched** - immunoprecipitated viral RNA-protein complexes bound to MyOne
613 C1 magnetic beads at the last washing step before protein elution. RNA was extracted from a 40
614 ul of cell lysate or bead suspension in the washing buffer representing each biological replicate
615 and subjected to Zika virus-specific RT-qPCR; dots represent ChIRP-MS biological replicates.
616 **(D)** The same nearly entire Zika RNA genome coverage and NGS depth in ZAP-WT and ZAP-
617 KO cells. Representative data from one ChIRP-MS biological replicate for ZAP-WT and ZAP-
618 KO cells. **Input** and **Enriched** are the same sample types as for RT-qPCR in **C**. Control NGS in
619 mock-infected cells did not show Zika-specific sequences (**Fig S4**). A red line shows the 10-
620 nucleotide NGS depth threshold.
621
622 **Fig 3. Top ChIRP-MS proteins and GO pathways identified in the Extended, ZAP-**
623 **independent, and ZAP-dependent Zika virus RNA interactomes.** Mean spectral counts are
624 shown for proteins in (**A**, **B**, **C**). Spectral counts for all three biological replicates are shown in
625 **Tables S1C, F, H**. The top proteins with unknown functions in RNA biology are highlighted in
626 grey. For GO pathways in (**D, E, F**), GO identification numbers and FDR-adjusted *P* values are
627 shown in parentheses. All GO processes were overrepresented.
628
629 **Fig 4. The expression of RNA helicases in VERO-ZAP-WT and VERO-ZAP-KO cells**. Cells
630 were mock infected or infected with normalized Zika virus MOIs; MOI 2 or 10 for VERO-ZAP-
631 KO and VERO-ZAP-WT cells, respectively, as described for ChIRP in supplemental materials
632 and methods. Cells were sampled at 72 h after mock or virus infection. (**A**) Green bands represent
633 DDX23 (96 kDa), DDX27 (90 kDa), DDX42 (117-120 kDa), and DDX50 (83 kDa) RNA

helicases. Red bands represent β-actin loading control (42 kDa). Western blot was done in 3 biological replicates for each experimental condition. (**B**) The expression of DDX RNA helicases was quantified as described in supplemental material and methods.

FIGURES

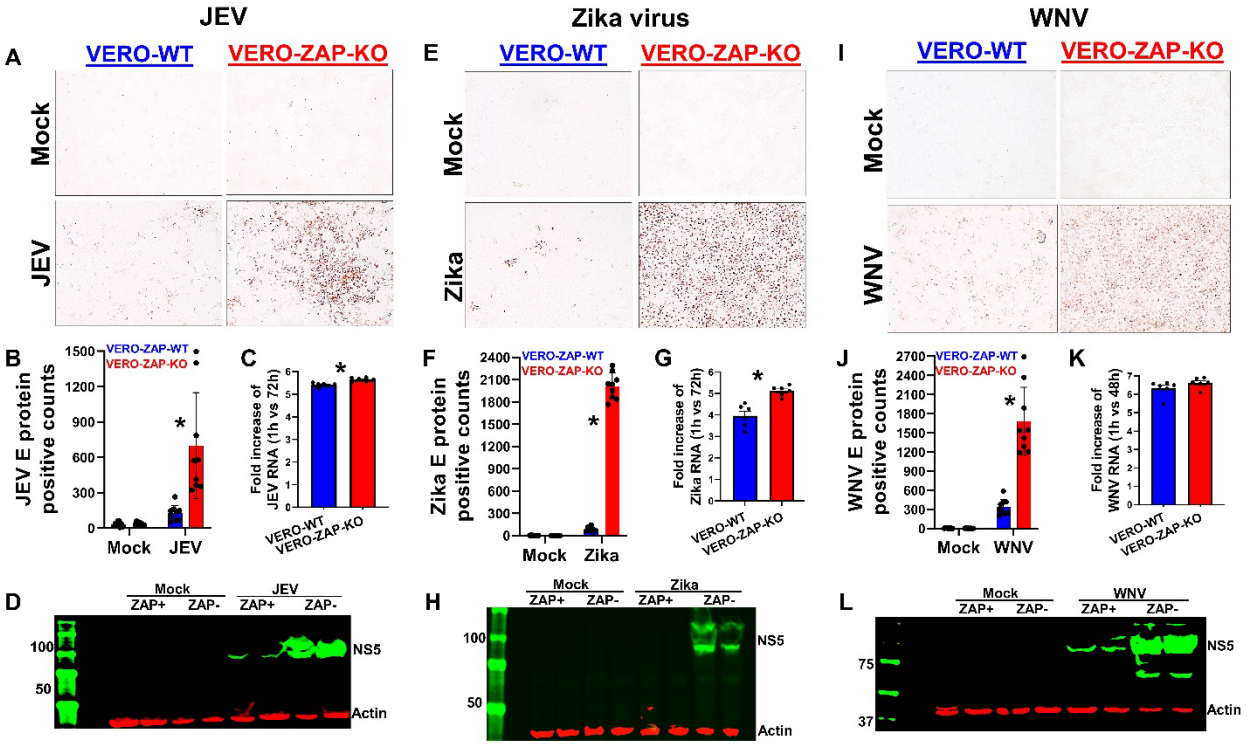

Fig 1.

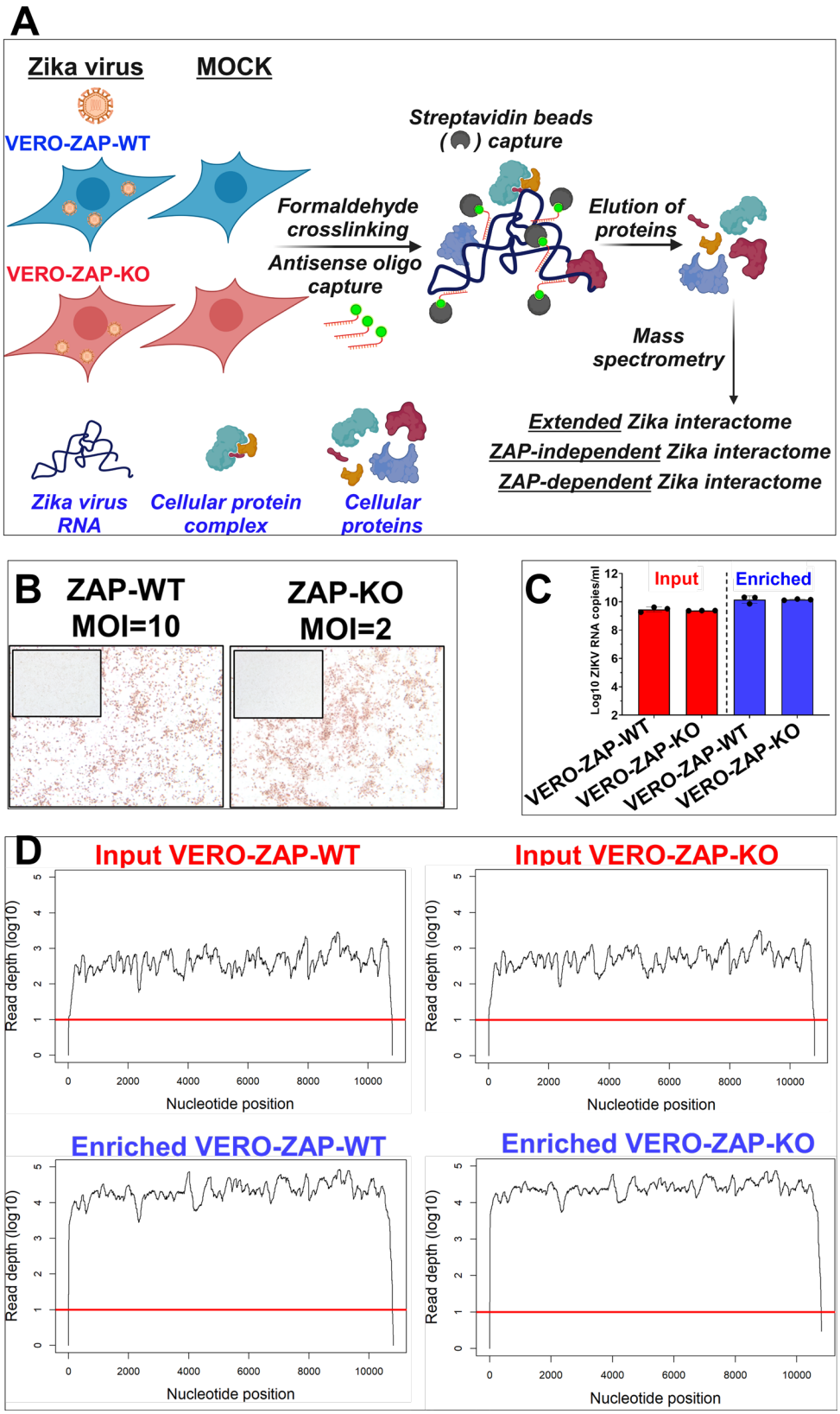
A
Zika virus
MOCK
VERO-ZAP-WT
VERO-ZAP-KO
Formaldehyde crosslinking
Antisense oligo capture
Streptavidin beads ( ) capture
Elution of proteins
Mass spectrometry
Extended Zika interactome
ZAP-independent Zika interactome
ZAP-dependent Zika interactome
Zika virus RNA
Cellular protein complex
Cellular proteins
B
ZAP-WT MOI=10
ZAP-KO MOI=2
C
Input
Enriched
Log10 ZIKV RNA copies/ml
VERO-ZAP-WT
VERO-ZAP-KO
VERO-ZAP-WT
VERO-ZAP-KO
D
Input VERO-ZAP-WT
Input VERO-ZAP-KO
Enriched VERO-ZAP-WT
Enriched VERO-ZAP-KO
Read depth (log10)
Nucleotide position

Fig 2.

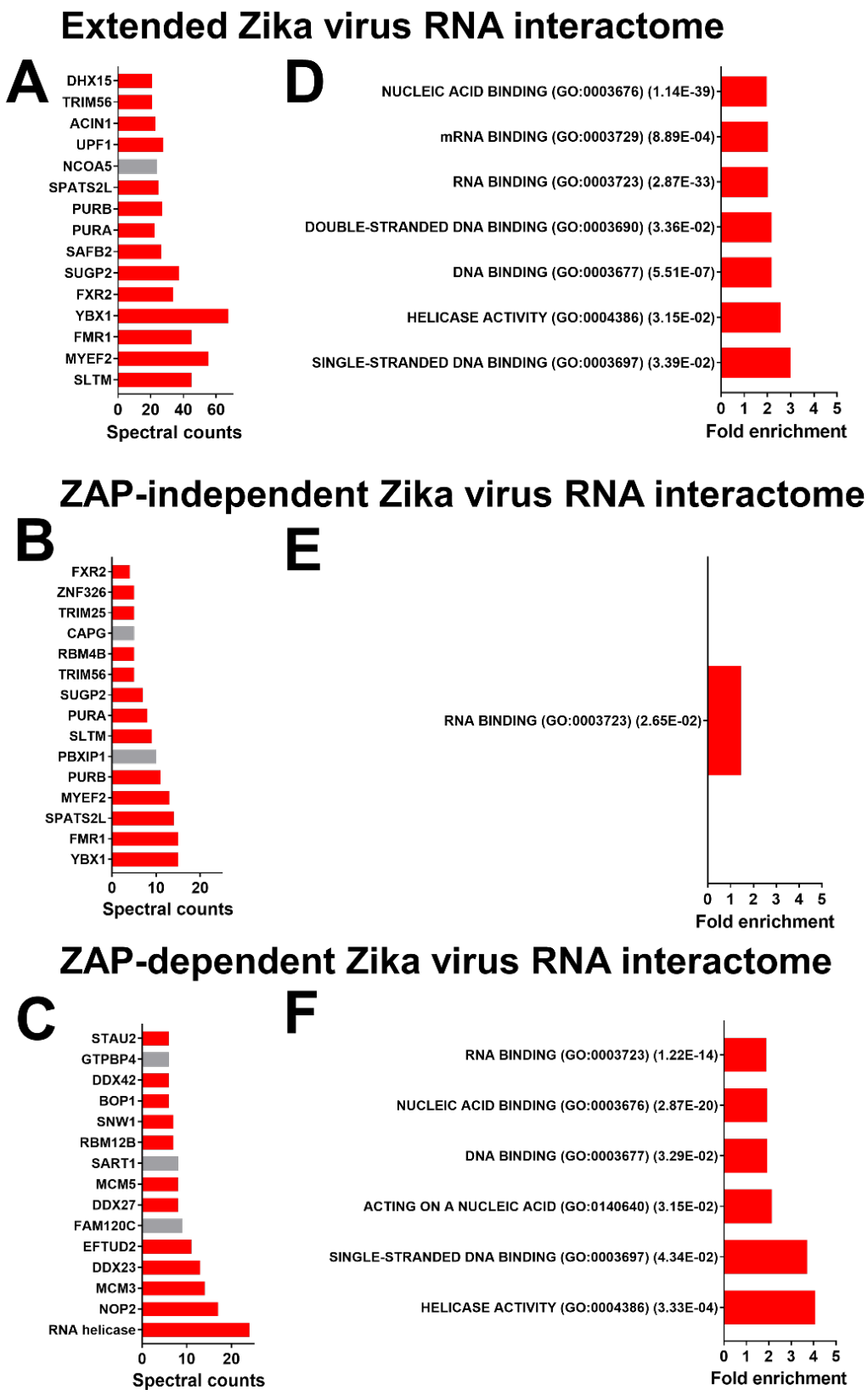
Extended Zika virus RNA interactome
A
DHX15
TRIM56
ACIN1
UPF1
NCOA5
SPATS2L
PURB
PURA
SAFB2
SUGP2
FXR2
YBX1
FMR1
MYEF2
SLTM
0 20 40 60
Spectral counts
D
NUCLEIC ACID BINDING (GO:0003676) (1.14E-39)
mRNA BINDING (GO:0003729) (8.89E-04)
RNA BINDING (GO:0003723) (2.87E-33)
DOUBLE-STRANDED DNA BINDING (GO:0003690) (3.36E-02)
DNA BINDING (GO:0003677) (5.51E-07)
HELICASE ACTIVITY (GO:0004386) (3.15E-02)
SINGLE-STRANDED DNA BINDING (GO:0003697) (3.39E-02)
0 1 2 3 4 5
Fold enrichment
ZAP-independent Zika virus RNA interactome
B
FXR2
ZNF326
TRIM25
CAPG
RBM4B
TRIM56
SUGP2
PURA
SLTM
PBXIP1
PURB
MYEF2
SPATS2L
FMR1
YBX1
0 10 20
Spectral counts
E
RNA BINDING (GO:0003723) (2.65E-02)
0 1 2 3 4 5
Fold enrichment
ZAP-dependent Zika virus RNA interactome
C
STAU2
GTPBP4
DDX42
BOP1
SNW1
RBM12B
SART1
MCM5
DDX27
FAM120C
EFTUD2
DDX23
MCM3
NOP2
RNA helicase
0 10 20
Spectral counts
F
RNA BINDING (GO:0003723) (1.22E-14)
NUCLEIC ACID BINDING (GO:0003676) (2.87E-20)
DNA BINDING (GO:0003677) (3.29E-02)
ACTING ON A NUCLEIC ACID (GO:0140640) (3.15E-02)
SINGLE-STRANDED DNA BINDING (GO:0003697) (4.34E-02)
HELICASE ACTIVITY (GO:0004386) (3.33E-04)
0 1 2 3 4 5
Fold enrichment

Fig 3.

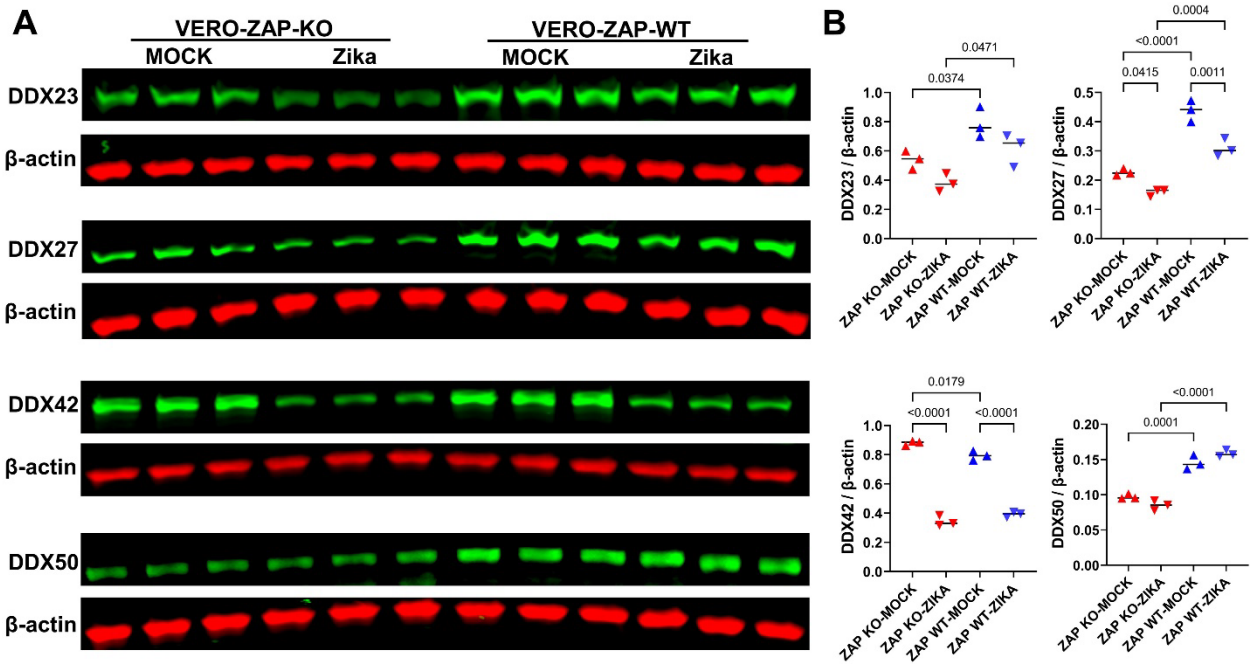
A
VERO-ZAP-KO
MOCK
Zika
VERO-ZAP-WT
MOCK
Zika
DDX23
β-actin
DDX27
β-actin
DDX42
β-actin
DDX50
β-actin
B
DDX23 / β-actin
0.0374
0.0471
DDX27 / β-actin
0.0415
<0.0001
0.0011
0.0004
DDX42 / β-actin
<0.0001
<0.0001
0.0179
DDX50 / β-actin
0.0001
<0.0001
ZAP KO-MOCK
ZAP KO-ZIKA
ZAP WT-MOCK
ZAP WT-ZIKA

Fig 4.

692 **SUPPORTING INFORMATION CAPTIONS**

693 **Supplemental Materials and Methods.** The file contains experimental details.
694
695
696 **Fig S1. Representative images of cells positive for flavivirus E protein (red staining) at 72 h**
697 **(JEV and Zika virus) and 48 h (WMV).** The experiment was done in 3 biological and 3 technical
698 replicates. All replicates are shown. MOI 0.01. The data from these replicate figures were used for
699 digital quantification in **Figs 1B**, **F**, **J**. (**A**) JEV in VERO-ZAP-WT cells. (**B**) JEV in VERO-ZAP-
700 KO cells. (**C**) Zika virus in VERO-ZAP-WT cells. (**D**) Zika virus in VERO-ZAP-KO cells. (**E**)
701 WNV in VERO-ZAP-WT cells. (**F**) WNV in VERO-ZAP-KO cells.
702
703 **Fig S2. VERO-ZAP-WT and VERO-ZAP-KO cells genotyped with Sanger sequencing as**
704 **described in Supplemental Materials and Methods.** Location of indels on *Chlorocebus sabaeus*
705 genome: -2bp deletion, NW_023666072.1: 4677550-4677551.
706
707 **Fig S3. ZAP Western blot. (A)** ZAP Western blot in VERO-ZAP-KO and VERO-ZAP-WT cells.
708 Cells were mock infected or infected with normalized Zika virus MOIs; MOI 2 or 10 for VERO-
709 ZAP-KO and VERO-ZAP-WT cells, respectively, as described for ChIRP in supplemental
710 materials and methods. Cells were sampled at 72 h after mock or virus infection. Green bands
711 represent ZAP with the manufacturer's predicted size 111 kDa; multiple bands may represent four
712 isoforms described for human ZAP [31] and still not experimentally characterized for monkeys.
713 Red bands represent β-actin loading control, 42 kDa. Western blot was done in 3 biological
714 replicates for each experimental condition. (**B**) The expression of ZAP was quantified as described
715 in supplemental material and methods.
716
717 **Fig S4. The Zika RNA genome coverage and NGS depth in VERO-ZAP-WT and VERO-**
718 **ZAP-KO cells**. **Input** - sonicated cellular lysates. **Enriched** - immunoprecipitated viral RNA-
719 protein complexes bound to MyOne C1 magnetic beads at the last washing step before protein
720 elution. Control NGS in mock-infected cells did not show Zika-specific sequences. A red line
721 shows the 10-nucleotide NGS depth threshold.
722
723
724 **Table S1-ChIRP-MS data**. The table contains raw and analyzed ChIRP-MS data. The table can
725 be accessed in the DRYAD open data publishing platform:
726 https://datadryad.org/stash/share/tqLeKFRU68c947MAFplLF9S8xrd_JM8IulT5JFSiEio
727
728
729 **Supplemental Dataset 1.** This dataset contains 26 raw fastq files representing paired-end NGS
730 data for **input** and **enriched** samples described in results, in **Figure 2D**, and in **Fig S4**. The
731 dataset also contains the "Zika virus NGS sample IDs" file which provides identifications for raw
732 files and experimental conditions (VERO-ZAP-WT or VERO-ZAP-KO cells; MOCK or Zika
733 virus; input or enriched samples; replicate number). The dataset can be accessed in the DRYAD
734 open data publishing platform:
735 https://datadryad.org/stash/share/GJWy9A9Hofp-9aya9oOLI9RgDsi_qqw6FITwPu4F0Gs

736

737 **Supplemental Dataset 2.** This dataset contains the folder "RAWfiles" with 12 Mass
738 spectrometry RAW data files representing three biological replicates for MOCK and Zika virus-
739 infected VERO-ZAP-WT and VERO-ZAP-KO cells. The folder "MSFragger" contains the
740 output of FragPipe v18.0 which was used to analyze Mass spectrometry RAW data files as
741 described in Supplemental Materials and Methods. The folder "MSFragger" contains data for
742 individual samples, and the "combined_protein.tsv" file (also represented in **Table S1B**), which
743 was used for the identification of Extended, ZAP-independent, and ZAP-dependent Zika virus
744 RNA interactomes from ChIRP-MS results as described in Supplemental Materials and Methods.
745 The "Zika virus ChIRP-MS sample IDs" file provides identifications for Mass spectrometry and
746 FragPipe raw files and experimental conditions (VERO-ZAP-WT or VERO-ZAP-KO cells;
747 MOCK or Zika virus; biological replicate number). The dataset can be accessed in the DRYAD
748 open data publishing platform:
749 https://datadryad.org/stash/share/GJWy9A9Hofp-9aya9oOLI9RgDsi_qqw6FITwPu4F0Gs

SUPPLEMENTAL MATERIALS AND METHODS

Endogenous ZAP affects Zika virus RNA interactome

Ahmad Jawad Sabir[1,a], Nguyen Phuong Khanh Le[2,a], Prince Pal Singh[2,3,a], Uladzimir Karniychuk[2,*]

[1]Department of Microbiology and Immunology, University of Illinois, College of Medicine, Chicago, IL, USA

[2]Department of Veterinary Biosciences, College of Veterinary Medicine, The Ohio State University, Columbus, OH, USA

[3]School of Public Health, University of Saskatchewan, Saskatoon, Canada

[a]**:** These authors contributed equally

*** Correspondence:** Uladzimir Karniychuk
Department of Veterinary Biosciences, College of Veterinary Medicine, The Ohio State University, Columbus, OH, USA
karniychuk.1@osu.edu

SUPPLEMENTAL MATERIALS AND METHODS

Cells

Wild-type and ZAP knockout VERO cells were previously described [1]. Briefly, wild-type VERO E6 cells (ATCC) (VERO-ZAP-WT) and ZAP knockout (VERO-ZAP-KO) derivatives were maintained in DMEM (Fisher, MA, USA; #11-965-118) supplemented with 10% heat-inactivated fetal bovine serum (FBS) (Fisher, MA, USA; #A5256801), 1x Penicillin-Streptomycin (Fisher, MA, USA; #15140122), and 2.67 mM sodium bicarbonate (Fisher, MA, USA; # 25080094) at +37°C in a 5% CO_2 humidified incubator. To generate Zinc finger CCCH-type antiviral protein 1 (ZAP) KO cell line, we used the guide RNA (gRNA) GTCTCTGGCAGTACTTGCGA which targets the first exon of *Chlorocebus sabaeus* (Gene ID: 103226990) ZC3HAV1 gene, which is required for the expression of all ZAP isoforms. A non-targeting control gRNA ACGGAGGCTAAGCGTCGCAA was also used. These gRNAs were transiently transfected into cells using GenCrispr NLS-Cas9-NLS Nuclease (GenScript). Transfected cells were plated in 96-well plates by limiting dilution to generate isogenic single clones. The clones were expanded and genotyped with Sanger sequencing; primers (F-ATCGCTGGGCTGGACTAACG, R-GCAGAGAAGGGAGTGGCTGAA) were used to identify indels (location of indels on *Chlorocebus sabaeus* genome: -2bp deletion, NW_023666072.1: 4677550-4677551; **Fig S2**). The knock-out subclone verified by genotyping was further confirmed by western blot [1] (**Fig S3**). The negative control cells were not isolated into single clones, but they were validated by Sanger sequencing to confirm there were no indels (**Fig S2**). Free mycoplasma contamination status in cells was confirmed using the LookOut Mycoplasma PCR Detection Kit (Millipore Sigma, MA, USA; #MP0035).

48 **Viruses**

49 We used the Asian lineage Zika virus H/PF/2013 strain. Zika virus was synthetically rescued
50 with reverse genetics in our previous study [2]; H/PF/2013 [GenBank: KJ776791.2] reference
51 sequence was used to rescue the virus. For JEV (SA14-14-2 strain, GenBank MK585066.1) and
52 WNV (NY99 strain, GenBank: DQ211652.1), we used the same reverse genetics system [2].
53 Viruses were propagated in VERO cells in DMEM supplemented with 2% FBS and 1%
54 penicillin/streptomycin (P/S). Supernatants were centrifuged (12,000 g, 20 min, +4°C),
55 aliquoted, and frozen (-80°C). Infectious virus titers were quantified using VERO E6 cells with
56 the endpoint dilution assay, and fifty percent tissue culture infective dose ($TCID_{50}$) endpoint
57 titers were calculated as previously described [2-5]. Media from virus-negative VERO cells was
58 processed in the same manner and used in control conditions. Free mycoplasma contamination
59 status in virus stocks was confirmed using the LookOut Mycoplasma PCR Detection Kit
60 (Millipore Sigma, MA, USA; #MP0035).

61

62 **Comparative infection phenotypes in wild-type and ZAP-KO cells infected with Zika virus,**
63 **JEV, and WNV**

64 We tested alongside JEV, Zika virus, and WNV in VERO-ZAP-WT and VERO-ZAP-KO cells.
65 Fifty thousand cells per well were seeded into 96-well plates; next day, media was removed, and
66 monolayers were inoculated with MOIs 0.01 of JEV, Zika, or WNV in 50 µl for 2 h at +37°C
67 and 5% CO_2. Afterward, the inoculum was removed and replaced with 150 µl DMEM
68 supplemented with 2% FBS, 1x Penicillin-Streptomycin, and 2.67 mM sodium bicarbonate. At 1
69 h and 72 h (48 h for WNV), cells in 9 wells representing three biological and three technical
70 replicates were fixed and stained for flavivirus E protein as we did [2,5-9]. For

71 immunohistochemistry staining we used 4G2 (ATCC, MA, USA; #HB-112) antibodies (Ab)
72 against Zika and WNV E protein, and #GTX125867 Ab (GeneTex, CA, USA) against JEV E
73 protein [2-5]. To quantify and compare immunohistochemistry staining between ZAP-WT and
74 ZAP-KO conditions, a magnification x200 images were randomly acquired in all replicates with
75 the same microscopic settings. Afterward each image was procced in ImageJ (NIH, USA) with
76 Automatic Particle counting (https://imagej.net/imaging/particle-analysis). In addition, cell
77 lysates from 3 biological and 2 technical replicates were collected at the same time points with
78 140 µl of PureLink RNA Mini Kit lyses buffer (Invitrogen) for subsequent RNA extraction and
79 virus-specific RT-qPCR [4,5,8,10]. The difference between ZAP-WT and ZAP-KO conditions
80 was represented by fold change of viral RNA loads in cell lysates collected at 1 h and 72 h (48 h
81 for WNV) after inoculation (1 h after inoculation was used to normalize for leftover virus
82 inoculum RNA).
83
84 **RNA extraction and virus-specific reverse transcriptase quantitative polymerase chain**
85 **reaction assays (RT-qPCR)**
86 To quantify intracellular Zika virus, JEV, and WNV RNA, total RNA was extracted from cell
87 lysates with PureLink RNA Mini Kit (Invitrogen) according to the manufacturer's instructions.
88 All RT-qPCR reactions were conducted on the Applied Biosystems QuantStudio 3 real-time
89 PCR system (Fisher, MA, USA) and analyzed using QuantStudio Design & Analysis Software
90 v1.5.2.
91
92 For Zika virus RNA quantification, we used the previously validated SYBR one-step RT-qPCR
93 assay [11]. The Luna Universal One-Step RT-qPCR Kit (NEB, MA, USA; # E3005L) reaction

94 mixture (20 µL) consisted of 10 µL Luna Universal One-Step Reaction Mix, 1 µL Luna
95 WarmStart RT Enzyme Mix, 1 µL (10 µM) of forward (ZIKV-F-SYBR: 5′-
96 AGGATCATAGGTGATGAAGAAAAGT-3′) and reverse (ZIKV−R-SYBR: 5′-
97 CCTGACAACACTAAGATTGGTGC-3′) primers, 3.4 µL nuclease-free water and 4 µL of RNA
98 template. The reverse transcription and enzyme activation steps of 10 min at 55˚C and 1 min at
99 95˚C were followed by 40 amplification cycles (10 s at 95˚C and 60 s at 60˚C). A standard curve
100 was generated and used to quantify Zika RNA loads as we described [1,2,4].
101
102 For JEV (F: 5′-GCCACCCAGGAGGTCCTT-3′; R: 5′-CCCCAAAACCGCAGGAAT-3′; Probe:
103 56-FAM-CAAGAGGTG/ZEN/GACGGCC-3IABkFQ) and WNV (F: 5′-
104 AGTAGTTCGCCTGTGTGAGC-3′; R: 5′-GCCCTCCTGGTTTCTTAGA-3′; Probe: 5’-FAM-
105 AATCCTCACAAACACTACTAAGTTTGTCA-TAMRA-3’), we used the previously validated
106 probe-based one-step RT-qPCR assays [12,13]. The Luna Universal Probe One-Step RT-qPCR
107 Kit reaction mixture (20 µL) consisted of 10 µL Luna Universal Probe One-Step Reaction Mix, 1
108 µL Luna WarmStart RT Enzyme Mix, 1 µL (10 µM) of forward and reverse primers, 0.5 µL of
109 the probe, 2.5 µL nuclease-free water and 4 µL of RNA template. The reverse transcription and
110 enzyme activation steps of 10 min at 55˚C and 1 min at 95˚C were followed by 40 amplification
111 cycles (10 s at 95˚C and 30 s at 60˚C). A standard curve was used to quantify viral RNA loads as
112 we described [1,2,4,6].
113
114 PCR values were corrected for volumes (140 µl of cell lyses buffer) and upon logarithmical
115 transformation expressed as virus RNA genome copies per mL. Strict precautions were taken to
116 prevent PCR contamination. All master mix preparations were done in the dedicated PCR

117 cabinet. Aerosol-resistant filter pipette tips and disposable gloves were used. Kit reagent controls
118 were included in every RNA extraction and PCR run.
119
120 **Western blot**
121 Cells in T-75 or T-175 flasks were washed, pelletized, and lysed in 150 or 300 µL of RIPA
122 buffer (Fisher, MA, USA; # PI89900) supplemented with 1× Halt protease inhibitor cocktail
123 (Fisher, MA, USA; # PI87786) and 1× EDTA (Fisher, MA, USA; #BP2482100). After 10
124 minutes of incubation on wet ice, the suspension was gently vortexed and centrifuged (12,000g,
125 10 min, +4 °C). Supernatants were aliquoted in prechilled low protein binding tubes and stored at
126 −80°C. After quantifying protein concentration with the Pierce BCA Protein Assay Kit (Fisher,
127 MA, USA; # PI23225), 50 µg of protein extract was mixed with 4x reducing Laemmli SDS
128 sample buffer (Fisher, MA, USA; # AAJ60015AC), boiled at 95ºC for 10 min, and resolved
129 using a 10% Mini-PROTEAN TGX precast protein gels (Bio-Rad, CA, USA; #4561036)
130 running in 1X Tris/Glycine/SDS running buffer (Bio-Rad, CA, USA; # 1610772) at a constant
131 current of 125V for 70 min. Proteins were transferred to methanol-activated 0.45 µm Immun-
132 Blot Low Fluorescence polyvinylidene fluoride (PVDF) (Bio-Rad, CA, USA; #1620260)
133 membranes using Trans-Blot Turbo RTA Mini 0.45µm LF PVDF Transfer Kit (Bio-Rad, CA,
134 USA; #1704274). Afterward, PVDF membranes were blocked with 1X VWR Life Science
135 Rapidblock Blocking Solution (VWR, GA, USA; #97064-124) for 1 h at room temperature. The
136 blocked membranes were incubated with primary antibody diluted in blocking solution overnight
137 at +4°C. Membranes were washed four times with TBST (1x Bio-Rad Tris Buffered Saline
138 containing 0.1% of Fisher Tween-20). After that, membranes were incubated with secondary
139 antibody along with hFAB™ Rhodamine Anti-Actin Primary Antibody (Recombinant human β-

140 actin) diluted in Blocking Solution for 1 h at room temperature, and washed four times with
141 TBST. Fluorescent blots were imaged on the ChemiDoc MP Imaging system (Bio-Rad, CA,
142 USA) using an appropriate detection channel with Image Lab Touch Software (Bio-Rad, CA,
143 USA).
144
145 We used antibodies (Abs): Rabbit anti-ZAP IgG Abs (1:1,000 dilution; ANTI-ZC3HAV1
146 #HPA059096-100UL, Millipore Sigma, MA, USA), Rabbit anti-DDX23 IgG Abs (1:1,000
147 dilution; #ab70461, Abcam, MA, USA), Rabbit anti-DDX27 IgG Abs (1:1,000 dilution;
148 #ab177938, Abcam, MA, USA), Rabbit anti-DDX42 IgG Abs (1:2,000 dilution; Fisher, MA, USA;
149 #A303-353A), Rabbit anti-DDX50 IgG Abs (1:1,000 dilution; #10358-1-AP; ProteinTech, IL,
150 USA), Rabbit anti-Zika virus NS5 IgG Abs (1:1,000 dilution; #GTX133312; GeneTex, CA, USA),
151 Rabbit anti-West Nile virus NS5 IgG Abs (1:1,500, #GTX131961; GeneTex, CA, USA), Rabbit
152 anti-Japanese Encephalitis virus NS5 Abs (1:1,500, #GTX131359; GeneTex, CA, USA), hFAB™
153 Rhodamine Anti-Actin Primary Abs (1:3,000; #12004164; Bio-Rad, CA, USA), and IRDye®
154 680RD Goat anti-Rabbit IgG secondary Abs (1:10,000; #926-68071; LI-COR, NE, USA).
155
156 Image Lab Software Version 6.1 (Bio-Rad, CA, USA) was used for Western blots densitometry
157 analysis according to the user guide instructions. Briefly, the "Lanes and Bands" option was used
158 to select the specific lanes and bands of the corresponding DDX RNA helicase, ZAP, and β-actin
159 lanes and bands. The "Lane Profile" option was used to subtract the background. In the "Analysis
160 Table," the background-adjusted (Adj. Volume) intensities of each DDX RNA helicase and ZAP
161 bands were normalized by the background-adjusted β-actin intensities. Subsequently, the DDX
162 RNA helicase (or ZAP)/β-actin ratios were used to analyze data for each experimental condition.

163 **Comprehensive Identification of RNA binding Proteins by Mass Spectrometry (ChIRP-**
164 **MS)**
165 We performed ChIRP-MS as described before [14-17]. Biotinylated DNA probes (**Table S2A**)
166 covering the whole Zika virus genome were designed using the online tool
167 (https://www.biosearchtech.com/chirp-designer). To have an even coverage of the whole
168 genome, 50 probes were designed by dividing the whole Zika reference sequence H/PF/2013
169 [GenBank: KJ776791.2] into two segments (1-5400 and 5401-10807), with a repeat masking
170 setting of 3 and spacing length of 80 (1 oligo around every 200 bp). Oligos were synthesized
171 with 3' biotin-TEG modification, final yield of 2 OD, and HPLC purification at Bio Basic Inc,
172 Canada. Fifty individual oligos were resuspended at 100 μM and mixed at equal volumes to
173 prepare the probe pool.
174
175 For Zika virus infection, VERO-ZAP-WT and VERO-ZAP-KO cells were seeded at 10^7 cells per
176 T-175 flask (4 flasks per experimental condition x 3 biological replicates) and were grown in
177 DMEM supplemented with 10% FBS. The next day, the media was removed, and cell
178 monolayers were washed with 1× PBS and inoculated with Zika virus at MOI 10 for VERO-
179 ZAP-WT cells and MOI 2 for VERO-ZAP-KO cells; these MOIs were adapted to provide the
180 same Zika virus loads. For this, we incrementally increased the MOI for VERO-ZAP-WT cells,
181 as Zika virus caused a more aggressive infection in VERO-ZAP-KO cells (**Figs 1E-H**). To
182 exclude the effects of differential uptake of the stimulus with MOI 10 in VERO-ZAP-WT cells,
183 during VERO-ZAP-KO MOI 2 Zika virus inoculation we added heat-inactivated virus equivalent
184 of MOI 8. Control cells were mock-treated with supernatant from virus-free control cells. Flasks
185 were incubated at 37°C for 2 h and gently shaken every 10 minutes. The inoculum from flasks

186 was removed, and monolayers were extensively washed with 1× PBS twice and 25 mL of
187 DMEM supplemented with 2% FBS was added to each flask.
188
189 After 72 h, for cell harvesting and chemical crosslinking, media was removed, cell monolayers
190 were rinsed with 1× PBS, trypsinized, washed, and cells from four T-175 flasks representing one
191 biological replicate were pooled for each experimental condition. Cells were cross-linked in 37
192 mL of 3% methanol free-formaldehyde (Fisher, MA, USA; #PI28908) diluted in 1× PBS and
193 incubated for 30 min at room temperature on a rotator. Afterwards, formaldehyde was quenched
194 with 3.7 mL of 1.25 M glycine (Fisher, MA, USA; #AAA1381636) with final concentration 125
195 mM and pelleted (2,000g, 5 min, +4°C). Cell pellets were washed, resuspended in 2.5ml of 1×
196 PBS, transferred to pre-weighed microcentrifuge tubes, and centrifuged (10,000g, 2 min, +4°C).
197 PBS was aspirated, tubes were placed on ice and weighted on an analytical scale to determine the
198 final pellet weight, snap frozen in liquid nitrogen, and stored at -80°C. Around 300 mg of cells
199 was obtained from four combined T-175 flasks (4 flasks per experimental condition x 3
200 biological replicates).
201
202 For cell lysis and sonication, cell pellets were thawed at RT, resuspended in the ChIRP lysis
203 buffer (50 mM Tris-HCl, pH 7.0, # BP1756500; 10 mM EDTA, #AAJ62786AK; 1% SDS, #
204 BP2436-200; all reagent are from Fisher, MA, USA) supplemented just before use with PMSF
205 (100 mM; #PI36978, Fisher, MA, USA; 10 µl per 1 ml of ChIRP lysis buffer), SUPERaseIn (20
206 U/ µl; #AM2694, Fisher, MA, USA; 10 ul per 1 ml of ChIRP lysis buffer), and protease inhibitor
207 (100x; #P178410, Fisher, MA, USA; 10 ul per 1 ml of ChIRP lysis buffer) to finally have 300
208 mg of cell pellet per 4 ml of the complete lysis buffer. The lysate from each sample were

209 aliquoted in 2 ml and sonicated using Sonics Ultrasonic Processor VCX750 with 3 mm microtip
210 at 20% amplitude with 15 seconds On, 45 seconds Off pulse intervals for 1 h (1 h for total 15 +
211 45 seconds On and Off intervals) in 15 mL MI Bioruptor Plus TPX Tubes (#C30010009;
212 HOLOGIC Diagenode, NJ, USA). The sonicated lysates were snap frozen in liquid nitrogen and
213 stored at -80°C until further use. Aliquots of sonicated lysates (40 µL) were used to extract
214 RNA/DNA with the Invitrogen PureLink RNA Mini Kit (#12-183-018A; Fisher, MA, USA)
215 according to manufacturer's instructions, and the efficiency of sonication was confirmed by
216 running extracts from all samples on 1% agarose gels. The average DNA/RNA length was
217 around 500 nucleotides in all samples. The RNA from these samples were also used for Zika-
218 specific RT-qPCR and Next Generation Sequencing (NGS) to analyze the entire Zika virus RNA
219 loads, genome coverage and NGS depth (see below and results).
220
221 For hybridization, sonicated lysates were thawed on ice and pre-cleaned by adding 30 µL washed
222 Invitrogen Dynabeads MyOne Streptavidin C1 (# 65001; Fisher, MA, USA) per 1 mL of lysate
223 and rotating at 37°C for 30 min in a hybridization oven. Beads were removed twice from lysates
224 using a magnetic stand; for this and all subsequent magnetic stand steps > 2 min magnetization
225 was applied before removing the supernatant. Next, for every 1 mL of pre-cleaned sonicated
226 lysate, 2 mL of ChIRP hybridization buffer (750 mM NaCl, 1% SDS, 50 mM Tris-HCl pH 7.0,
227 1 mM EDTA, 15% formamide supplemented with PMSF, SUPERaseIn, and protease inhibitor as
228 described above for lysis buffer) and 2.5 µL of the 100 µM ChIRP probe pool were added. In our
229 experiments, the total volume of pre-cleaned sonicated lysate and ChIRP hybridization buffer
230 was 12 ml per sample; for efficient hybridization, we distributed each sample in 6 ml aliquots
231 and rotated in the hybridization over for 16 h at 37°C.

232 For enrichment of hybridized Zika virus RNA and associated proteins, per 1 mL of the initial
233 sample, 250 µL of washed (washed 3 times in un-supplemented lysis buffer) Dynabeads MyOne
234 Streptavidin C1 was added in each sample (in our study, 1 ml of beads was added per initial 4 ml
235 lysis buffer sample), and rotated in the hybridization oven for 45 min at 37°C. Two 15 ml tubes
236 representing one sample were placed on the magnetic stand, supernatants were removed, and
237 beads were combined in 1 ml of ChIRP wash buffer (2x SSC, #AAJ60561AP, Fisher, MA, USA;
238 0.5% SDS supplemented with 1 mM PMSF just before use) in 1.5 ml low-binding Eppendorf
239 tube. Afterward, beads were washed 5 times in 1 ml of the ChIRP wash buffer by rotating at
240 37°C for 5 min in the hybridization oven, placing for 4 min on the magnetic stand, and replacing
241 the wash buffer. During the final wash, 10 µL of beads in the wash buffer were collected for
242 RNA extraction, Zika-specific RT-qPCR and NGS to analyze the Zika RNA loads, entire virus
243 genome coverage and NGS depth (see below and results).
244
245 For elution, beads were collected on the magnetic stand, resuspended in 600 µL of the ChIRP
246 biotin elution buffer (12.5 mM biotin # B20656; 7.5 mM HEPES pH 7.9, #AAJ61275AK;
247 75 mM NaCl, # NC1071140; 1.5 mM EDTA, 0.15% SDS, 0.075% sarkosyl, # NC1386335; and
248 0.02% Sodium deoxycholate, #AAB2075914; all reagent are from Fisher, MA, USA), rotated at
249 25°C for 20 min, and at 65°C for 15 min. Beads were placed on the magnetic stand and eluents
250 were transferred to a fresh tube, and beads were eluted again with 600 µL of the ChIRP biotin
251 elution buffer. The two eluents were pooled (final 1200 µL) and residual beads were removed
252 again using the magnetic stand. Afterward, 300 µL of trichloroacetic acid (#T0699; Millipore
253 Sigma, MA, USA) (25% of the final elute volume) was added to the clean eluent, vortexed, and
254 placed at 4°C overnight for precipitation. The next day, proteins were pelleted at 21,000 g at 4°C

255 for 45 min. Supernatants were carefully removed, and protein pellets were washed once with ice-
256 cold acetone (#A18-1; Fisher, MA, USA). Samples were spun at 21,000 g at 4°C for 5 min.
257 Acetone was removed, tubes briefly centrifuged again and after removal of residual acetone
258 tubes were left to air-dry for 1 minute. Then, 60 µL of preheated 1× ChIRP lysis buffer
259 containing 50 mM TEAB (# PI90114; Fisher, MA, USA) and 5% SDS (# BP2436-200; Fisher,
260 MA, USA) were added to the protein pellet and gently mixed several times with 200 µL pipette
261 tips. Samples were immediately put on dry ice and stored in -80°C until sent to the proteomics
262 facility.
263
264
265 To validate the same viral RNA loads in all samples/experimental conditions at the time of
266 formaldehyde RNA-protein fixation and ChIRP, RNA extracted during cell lysis (**input**) and
267 elution steps (**enriched**) (see above) were tested with Zika virus-specific RT-qPCR assay and
268 NGS to analyze the entire Zika virus genome coverage and NGS depth (**Supplemental Dataset**
269 **1**). The Zika virus-specific RT-qPCR assay was conducted as described above. For NGS,
270 samples were brought to the final volume of 50 µL with 1x PBS and 5 µL Proteinase K
271 (#FEREO0491; Fisher, MA, USA) and incubated at 55˚C for 30 minutes. Then, RNA was
272 extracted with the RNA Clean & Concentrator-5 Research Kit (ZYMO) and treated with the
273 Invitrogen TURBO DNA-free Kit (#AM1907; Fisher, MA, USA). Afterward, 7 µL of RNA was
274 used to produce cDNA with the Maxima H Minus First Strand cDNA Synthesis Kit
275 (#FERK1652; Fisher, MA, USA) and random hexamers, following the manufacturer's
276 instructions. The single stranded cDNA (20 µL) was further used to prepare double-stranded
277 DNA (dsDNA) using the NEBNext® Second Strand Synthesis (dNTP-free) Reaction Buffer

278 (#B6117S; NEB, MA, USA) mixed with the DNA Polymerase I (#M0209S; NEB, MA, USA),
279 E. coli DNA Ligase (#M0205S; NEB, MA, USA), RNase H (#M0297S; NEB, MA, USA),
280 random hexamers (#N8080127; Fisher, MA, USA), and dNTPs mix (#18427088; Fisher, MA,
281 USA). The dsDNA was used for library construction with the NEBNext® Ultra II DNA Library
282 Prep Kit for Illumina (#E7645L; NEB, MA, USA) and NEBNext® Multiplex Oligos for
283 Illumina® (96 Index Primers) (#E6609S; NEB, MA, USA) as we previously described [7,18,19].
284 Briefly, the libraries were constructed according to the manufacturer's instructions, with 1:10
285 adaptor dilution (volume of adaptor:total volume), and following cleanup step of adaptor-ligated
286 DNA without size selection. Individual libraries were quantified using Qubit dsDNA HS Assay
287 Kit (#Q32856; Fisher, MA, USA) and Qubit 4.0 Fluorometer (Fisher, MA, USA). The peak size
288 of the libraries was confirmed with the Agilent DNA 1,000 kit on Agilent 2100 Bioanalyzer
289 (Agilent, CA, USA). Afterward, 20 ng of each barcoded library were pooled, quantified (Qubit),
290 quality-checked (Agilent Bioanalyzer), and converted to moles: Molecular weight [nM] =
291 Library concentration [ng/µL] / (Average library size x 650)/1,000,000). The pooled library was
292 diluted to 2 nM in 10 mM TE buffer, denatured with 0.1 N NaOH, diluted to 14 pM, and paired-
293 end 300 nt reads were generated with the MiSeq Reagent kit v3 600 cycle output (Illumina, CA,
294 USA) on the MiSeq System (Illumina, CA, USA). To compare Zika virus RNA coverage and
295 NGS depth, FASTQ files representing different samples/experimental conditions were trimmed
296 for adaptor sequences and filtered for low-quality reads using Trimmomatic. Next, the trimmed
297 FASTQ paired files were aligned to the Zika virus reference sequence H/PF/2013 [GenBank:
298 KJ776791.2] using Burrows-Wheeler Aligner (BWA) [20] and output BAM files were used to
299 quantify and visualize the virus genome coverage and NGS depth with the in-house R script
300 (https://github.com/itrus/bash-scripts-NGS/tree/main) [7,18,19].

301

302 Preparation and mass spectrometry analysis of ChIRP samples were done in The Proteomics
303 Facility, Network Biology Collaborative Centre, Lunenfeld-Tanenbaum Research Institute,
304 Toronto. For the S-Trap (ProtiFi, NY, USA) [21,22] the whole volume containing ChIRP-
305 precipitated proteins were used. The material was reduced with 20 mM DTT for 10 minutes at
306 +95°C and alkylated with 40 mM iodoacetamide for 30 minutes in the dark. Phosphoric acid was
307 added to achieve a final concentration of 1.2%. To each 27.5 µl of acidified lysate, 165 µl of S-
308 Trap protein binding buffer (90% methanol, 100 mM TEAB) was added. The resulting mixture
309 was passed through the micro column at 4,000 × g, and the column was washed four times with
310 the S-Trap protein binding buffer. Each sample was digested with 1 µg of trypsin (in 20 µl of 50
311 mM TEAB) for 1 hour at +47°C. Prior to elution, 40 µl of 50 mM TEAB (pH 8) was added to
312 the column. Peptides were eluted by centrifugation at 4,000 × g. Peptides were eluted two more
313 times with 40 µl of 2% formic acid and 40 µl of 50% acetonitrile + 2% formic acid. Eluted
314 peptides were dried down and stored at -40°C.

315

316 For data-dependent acquisition (DDA) LC-MS/MS, digested peptides were analyzed using a
317 nano-HPLC coupled to MS. Half of the sample was used for DDA. Coated Nano-spray emitters
318 were generated from fused silica capillary tubing, with 75µm internal diameter, 365µm outer
319 diameter and 5-8µm tip opening, using a laser puller (Sutter Instrument Co., model P-2000, with
320 parameters set as heat: 280, FIL = 0, VEL = 18, DEL = 2000). Nano-spray emitters were packed
321 with C18 reversed-phase material (Reprosil-Pur 120 C18-AQ, 1.9 µm) resuspended in methanol
322 using a pressure injection cell. The sample in 5% formic acid was directly loaded at 400 nl/min
323 onto a 75 µm x 15 cm nano-spray emitter. Peptides were eluted from the column with an

324 acetonitrile gradient generated by an Vanquish Neo UHPLC System and analyzed on an Orbitrap
325 Fusion Lumos Tribrid. The gradient was delivered at 200 nl/min from 3.2% acetonitrile with
326 0.1% formic acid to 35.2% acetonitrile with 0.1% formic acid using a linear gradient of 90
327 minutes. This was followed by a 3 min gradient from 35.2% acetonitrile with 0.1% formic acid
328 to 79.2% acetonitrile with 0.1% formic acid. Afterward, there was a 5.8 min wash with 79.2%
329 acetonitrile with 0.1% formic acid, and the column was equilibrated at 400nl/min for 6.4min.
330 The total DDA protocol was 99 minutes. The MS1 scan had an accumulation time of 50 ms
331 within a mass range of 400–1500Da, using orbitrap resolution of 120000, 60% RF lens, AGC
332 target of 125% and 2400 volts. This was followed by MS/MS scans with a total cycle time of 3
333 seconds. Accumulation time of 50 ms and 33% HCD collision energy was used for each MS/MS
334 scan. Each candidate ion was required to have a charge state from 2-7 and an AGC target of
335 400%, isolated using an orbitrap resolution of 15,000. Previously analyzed candidate ions were
336 dynamically excluded for 9 seconds.
337
338 Mass spectrometry RAW data files (**Supplemental Dataset 2**) were converted using
339 ThermoRawFileParser GUI -V 1.7.1 (https://github.com/compomics/ThermoRawFileParserGUI)
340 to the mzML format compatible with FragPipe. The RAW files were analyzed using FragPipe
341 v18.0 (**Supplemental Dataset 2**), which utilized MSFragger v3.5, Philosopher v4.4.0, and
342 IonQuant for peptide searching in the raw files [23-25]. The LFQ-MBR workflow was used, with
343 the *Chlorocebus sabaeus* Proteome ID UP000029965
344 (https://www.uniprot.org/proteomes/UP000029965) database with appended Zika virus
345 H/PF/2013 [GenBank: KJ776791.2], decoys, and contaminants sequences. Data from the output

346 “combined_protein.tsv” file (**Table S1B; Supplemental Dataset 2**) were used for interactome
347 analysis described below.
348
349 **Identification of Extended, ZAP-independent, and ZAP-dependent Zika virus RNA**
350 **interactomes from ChIRP-MS results**
351 The Zika virus RNA-interacting proteins were scored with the Mass spectrometry interaction
352 STatistics (MiST) analysis which was previously applied for ChIRP-MS [17,26,27]. We used
353 MiST default parameters; for specificity, we also selected the Singleton Filtering MiST option to
354 exclude proteins with spectral counts in only one biological replicate and quantify proteins with
355 MiST score 0.75 or above [17,26,27]. We also excluded all proteins which had at least a single
356 spectral count in at least one of biological replicate in mock-infected wild-type or ZAP-KO cells
357 [17,28].
358
359 We applied three analytical strategies to examine ChIRP-MS data. For the first analytical
360 strategy, using the raw ChIRP-MS data with total 2,269 proteins (**Table S1B)**, we identified
361 proteins specifically associated with Zika virus RNA in VERO-ZAP-WT cells. We defined the
362 resultant list of enriched proteins as “extended” Zika virus RNA interactome in VERO-ZAP-WT
363 cells. For the second analytical strategy, we identified proteins specifically interacting with Zika
364 virus RNA in VERO-ZAP-KO cells. We defined the resultant list of enriched proteins as “ZAP-
365 independent” Zika virus RNA interactome. We defined this interactome as ZAP-independent
366 because associated cellular proteins were discovered in VERO-ZAP-KO cells which shows
367 ZAP-independent nature of interactions. Finally, for the discovery of “ZAP-dependent” Zika
368 RNA interactome in VERO-ZAP-WT cells, in addition to the above specificity exclusion criteria

369 in MiST settings and in mock-infected cells, we excluded proteins which had at least one spectral
370 count in at least one of the biological replicates in VERO-ZAP-KO cells infected with Zika
371 virus.
372 For ZAP-independent and ZAP-dependent Zika virus RNA interactomes, we performed GO
373 enrichment analyses of the identified proteins using The Gene Ontology Resource
374 (https://geneontology.org/) which connects to the analysis tool from the PANTHER
375 Classification System [29-31]. For analysis, GO aspect molecular function was selected. As
376 recommended, a custom reference list containing all proteins' IDs identified in the specific mass
377 spectrometry run (**Tables S1B**) was added after initial analysis on The Gene Ontology Resource
378 and the analysis was re-run on the PANTHER website. The significance *P* values of GO terms
379 were calculated by Fisher's exact test and adjusted by FDR.
380
381 **Statistics**
382 We used GraphPad PRISM 9 software. For the comparison of the number of virus-positive cell
383 counts, and viral RNA loads between wild-type and ZAP-KO cells we used an unpaired t-test.
384 For the comparison of Western blot protein expression, we used one-way ANOVA multiple
385 comparisons. P-value < 0.05 was considered statistically significant.
386
387
388

389 **SUPPLEMENTAL REFERENCES**

390 1. Nguyen Phuong Khanh Le PPS, Ahmad Jawad Sabir, Ivan Trus, Uladzimir Karniychuk. Endogenous
391 ZAP is associated with altered global cellular gene expression during Zika virus infection. bioRxiv.
392 2024. https://doi.org/10.1101/2024.05.23.595518
393 2. Trus I, Udenze D, Berube N, et al. CpG-Recoding in Zika Virus Genome Causes Host-Age-
394 Dependent Attenuation of Infection With Protection Against Lethal Heterologous Challenge in
395 Mice. Front Immunol. 2019;10:3077.
396 3. Trus I, Berube N, Jiang P, et al. Zika Virus with Increased CpG Dinucleotide Frequencies Shows
397 Oncolytic Activity in Glioblastoma Stem Cells. Viruses: Multidisciplinary Digital Publishing
398 Institute; 2020. p. 579.
399 4. Udenze D, Trus I, Berube N, et al. The African strain of Zika virus causes more severe in utero
400 infection than Asian strain in a porcine fetal transmission model. Emerging Microbes &
401 Infections. 2019; 8:1098-1107.2019.
402 5. Darbellay J, Cox B, Lai K, et al. Zika Virus Causes Persistent Infection in Porcine Conceptuses and
403 may Impair Health in Offspring. EBioMedicine. 25:73-86.2017.
404 6. Chapagain S, Pal Singh P, Le K, et al. Japanese encephalitis virus persists in the human
405 reproductive epithelium and porcine reproductive tissues. PLoS Negl Trop Dis. 2022
406 Jul;16(7):e0010656.
407 7. Sabir AJ, Singh PP, Trus I, et al. Asian Zika virus can acquire generic African-lineage mutations
408 during in utero infection. Emerg Microbes Infect. 2023 Dec;12(2):2263592.
409 8. Darbellay J, Lai K, Babiuk S, et al. Neonatal pigs are susceptible to experimental Zika virus
410 infection. Emerg Microbes Infect. 2017 Feb 15;6(2):e6.
411 9. Trus I, Udenze D, Cox B, et al. Subclinical in utero Zika virus infection is associated with
412 interferon alpha sequelae and sex-specific molecular brain pathology in asymptomatic porcine
413 offspring. In: Pierson TC, editor. PLoS Pathogens2019. p. e1008038.
414 10. Trus I, Darbellay J, Huang Y, et al. Persistent Zika virus infection in porcine conceptuses is
415 associated with elevated in utero cortisol levels. Virulence2018. p.
416 21505594.2018.1504558.
417 11. Xu MY, Liu SQ, Deng CL, et al. Detection of Zika virus by SYBR green one-step real-time RT-PCR.
418 Journal of virological methods: J Virol Methods; 2016. p. 93-97.
419 12. Eiden M, Vina-Rodriguez A, Hoffmann B, et al. Two new real-time quantitative reverse
420 transcription polymerase chain reaction assays with unique target sites for the specific and
421 sensitive detection of lineages 1 and 2 West Nile virus strains. J Vet Diagn Invest. 2010
422 Sep;22(5):748-53.
423 13. Shao N, Li F, Nie K, et al. TaqMan Real-time RT-PCR Assay for Detecting and Differentiating
424 Japanese Encephalitis Virus. Biomedical and environmental sciences : BES: Biomed Environ Sci;
425 2018. p. 208-214.
426 14. Chu C, Zhang QC, da Rocha ST, et al. Systematic discovery of Xist RNA binding proteins. Cell.
427 2015 Apr 9;161(2):404-16.
428 15. Flynn RA, Belk JA, Qi Y, et al. Discovery and functional interrogation of SARS-CoV-2 RNA-host
429 protein interactions. Cell. 2021 Apr 29;184(9):2394-2411 e16.
430 16. Ooi YS, Majzoub K, Flynn RA, et al. An RNA-centric dissection of host complexes controlling
431 flavivirus infection. Nat Microbiol. 2019 Dec;4(12):2369-2382.
432 17. Zhang S, Huang W, Ren L, et al. Comparison of viral RNA-host protein interactomes across
433 pathogenic RNA viruses informs rapid antiviral drug discovery for SARS-CoV-2. Cell Res. 2022
434 Jan;32(1):9-23.

435 18. Udenze D, Trus I, Berube N, et al. CpG content in the Zika virus genome affects infection
436 phenotypes in the adult brain and fetal lymph nodes. Front Immunol. 2022;13:943481.
437 19. Udenze D, Trus I, Munyanduki H, et al. The isolated in utero environment is conducive to the
438 emergence of rna and dna virus variants. Viruses: Multidisciplinary Digital Publishing Institute;
439 2021. p. 1827.
440 20. Li H, Durbin R. Fast and accurate short read alignment with Burrows-Wheeler transform.
441 Bioinformatics. 2009 Jul 15;25(14):1754-60.
442 21. Bang G, Lee H, Kim H, et al. Comparison of protein characterization using In solution and S-Trap
443 digestion methods for proteomics. Biochem Biophys Res Commun. 2022 Jan 22;589:197-203.
444 22. HaileMariam M, Eguez RV, Singh H, et al. S-Trap, an Ultrafast Sample-Preparation Approach for
445 Shotgun Proteomics. J Proteome Res. 2018 Sep 7;17(9):2917-2924.
446 23. Yu F, Haynes SE, Teo GC, et al. Fast Quantitative Analysis of timsTOF PASEF Data with MSFragger
447 and IonQuant. Mol Cell Proteomics. 2020 Sep;19(9):1575-1585.
448 24. da Veiga Leprevost F, Haynes SE, Avtonomov DM, et al. Philosopher: a versatile toolkit for
449 shotgun proteomics data analysis. Nat Methods. 2020 Sep;17(9):869-870.
450 25. Kong AT, Leprevost FV, Avtonomov DM, et al. MSFragger: ultrafast and comprehensive peptide
451 identification in mass spectrometry-based proteomics. Nat Methods. 2017 May;14(5):513-520.
452 26. Verschueren E, Von Dollen J, Cimermancic P, et al. Scoring Large-Scale Affinity Purification Mass
453 Spectrometry Datasets with MiST. Curr Protoc Bioinformatics. 2015 Mar 9;49:8 19 1-8 19 16.
454 27. Jager S, Cimermancic P, Gulbahce N, et al. Global landscape of HIV-human protein complexes.
455 Nature. 2011 Dec 21;481(7381):365-70.
456 28. Goodier JL, Pereira GC, Cheung LE, et al. The Broad-Spectrum Antiviral Protein ZAP Restricts
457 Human Retrotransposition. PLOS Genetics: Public Library of Science; 2015. p. e1005252.
458 29. The Gene Ontology C. Expansion of the Gene Ontology knowledgebase and resources. Nucleic
459 Acids Res. 2017 Jan 4;45(D1):D331-D338.
460 30. Mi H, Muruganujan A, Huang X, et al. Protocol Update for large-scale genome and gene function
461 analysis with the PANTHER classification system (v.14.0). Nat Protoc. 2019 Mar;14(3):703-721.
462 31. Mi H, Muruganujan A, Ebert D, et al. PANTHER version 14: more genomes, a new PANTHER GO-
463 slim and improvements in enrichment analysis tools. Nucleic Acids Res. 2019 Jan 8;47(D1):D419-
464 D426.

465

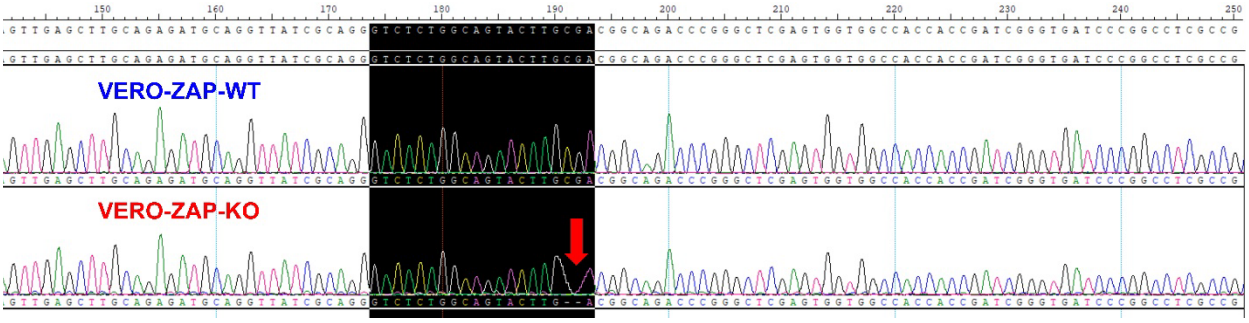

Fig S2. VERO-ZAP-WT and VERO-ZAP-KO cells genotyped with Sanger sequencing as described in Supplemental Materials and Methods. Location of indels on *Chlorocebus sabaeus* genome: -2bp deletion, NW_023666072.1: 4677550-4677551.

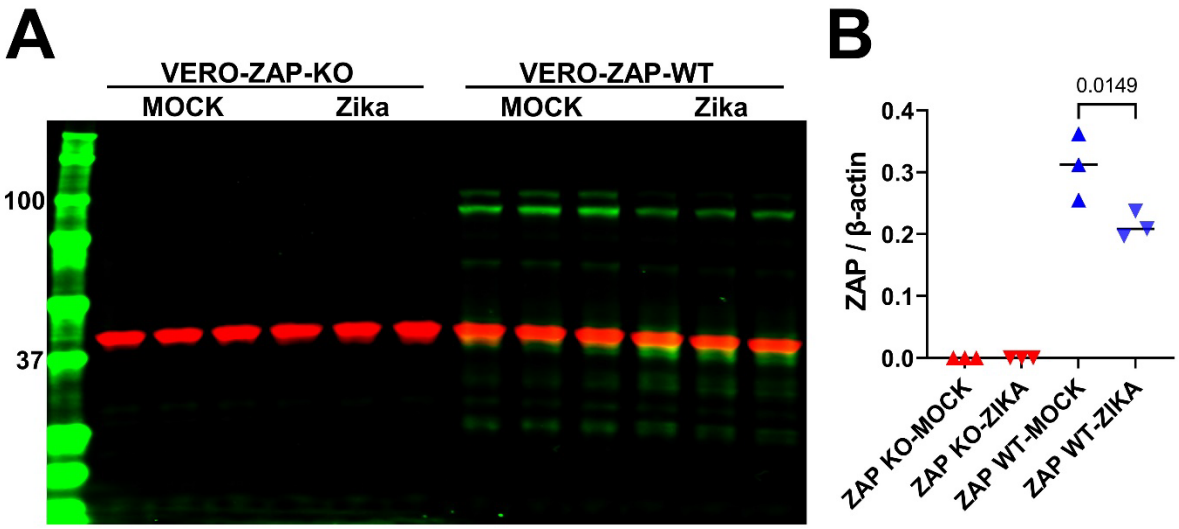

Fig S3. ZAP Western blot. (A) ZAP Western blot in VERO-ZAP-KO and VERO-ZAP-WT cells. Cells were mock infected or infected with normalized Zika virus MOIs; MOI 2 or 10 for VERO-ZAP-KO and VERO-ZAP-WT cells, respectively, as described for ChIRP in supplemental materials and methods. Cells were sampled at 72 h after mock or virus infection. Green bands represent ZAP with the manufacturer's predicted size 111 kDa; multiple bands may represent four isoforms described for human ZAP [1] and still not experimentally characterized for monkeys. Red bands represent β-actin loading control, 42 kDa. Western blot was done in 3 biological replicates for each experimental condition. (**B**) The expression of ZAP was quantified as described in supplemental material and methods.

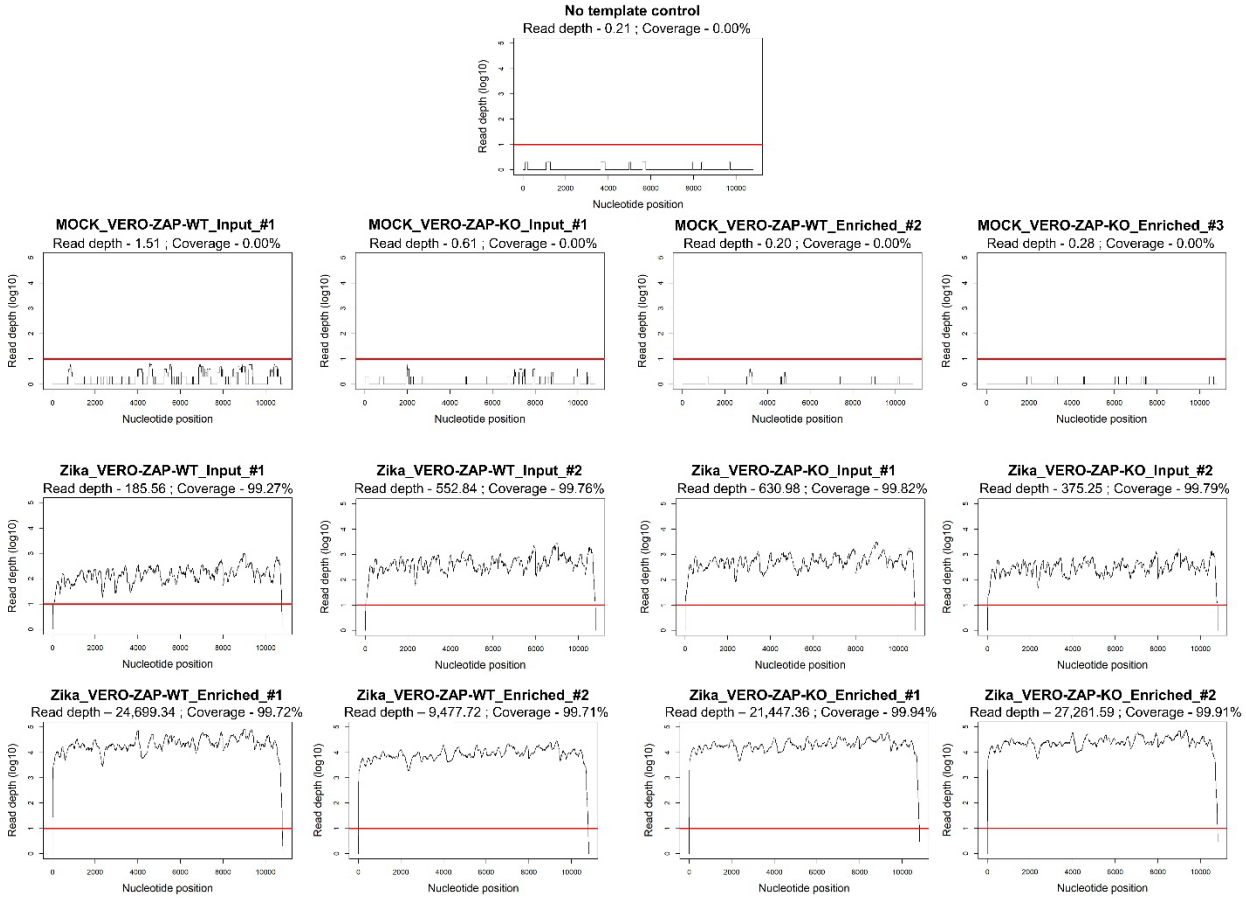

Fig S4. The Zika RNA genome coverage and NGS depth in VERO-ZAP-WT and VERO-ZAP-KO cells. **Input** - sonicated cellular lysates. **Enriched** - immunoprecipitated viral RNA-protein complexes bound to MyOne C1 magnetic beads at the last washing step before protein elution. Control NGS in mock-infected cells did not show Zika-specific sequences. A red line shows the 10-nucleotide NGS depth threshold.

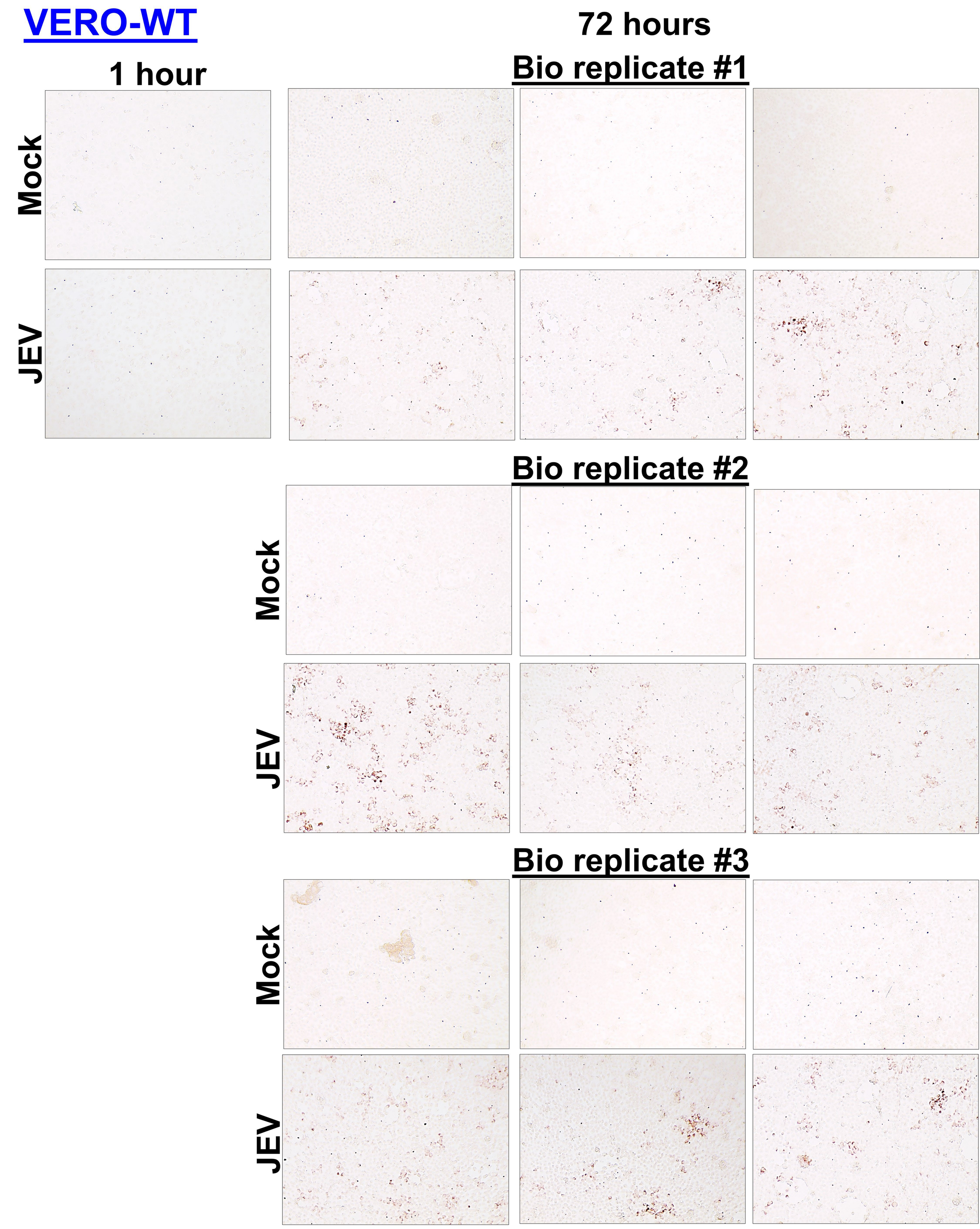
VERO-WT
1 hour
72 hours
Bio replicate #1
Mock
JEV
Bio replicate #2
Mock
JEV
Bio replicate #3
Mock
JEV

S1FigA

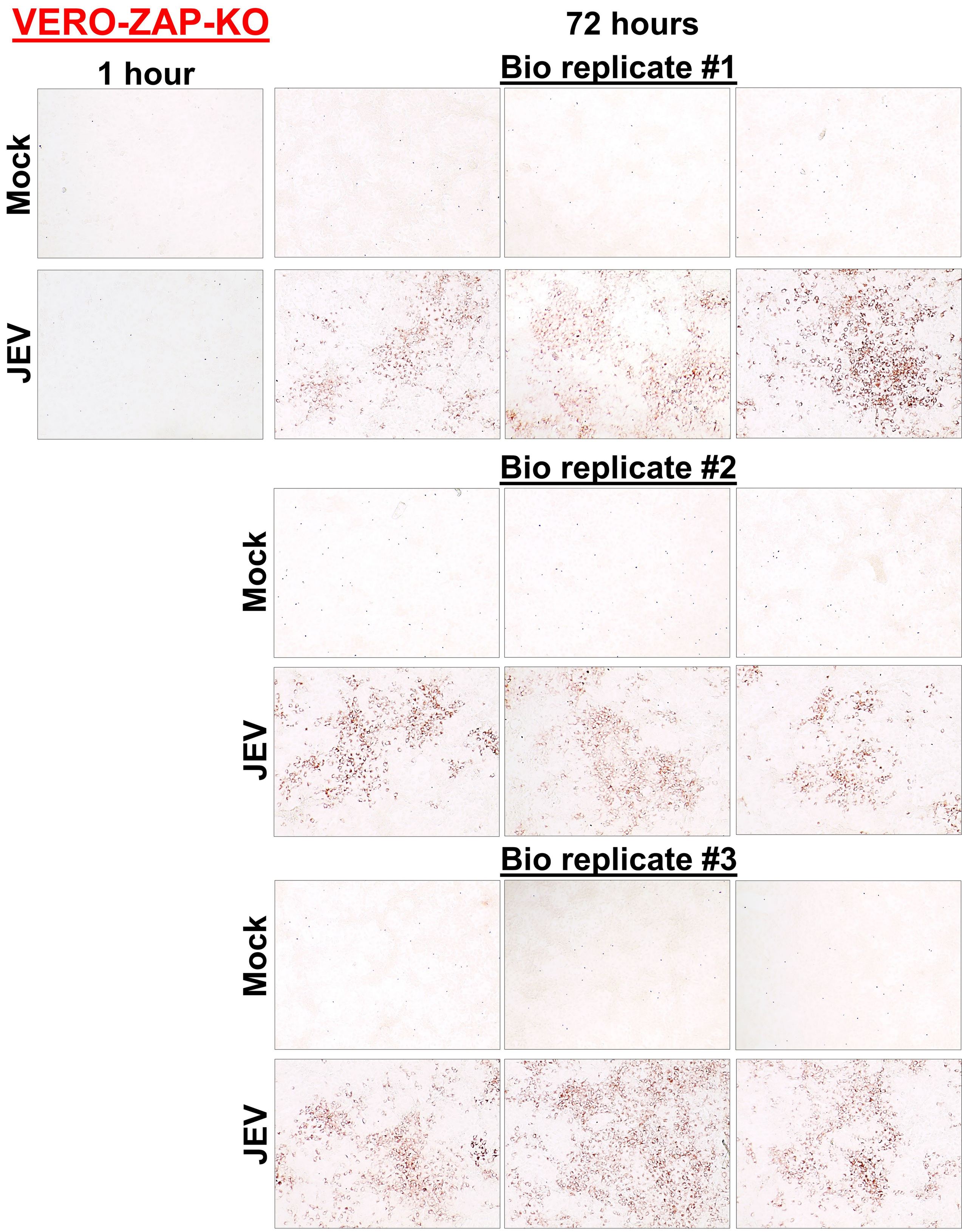
VERO-ZAP-KO
1 hour
72 hours
Bio replicate #1
Mock
JEV
Bio replicate #2
Mock
JEV
Bio replicate #3
Mock
JEV

S1FigB

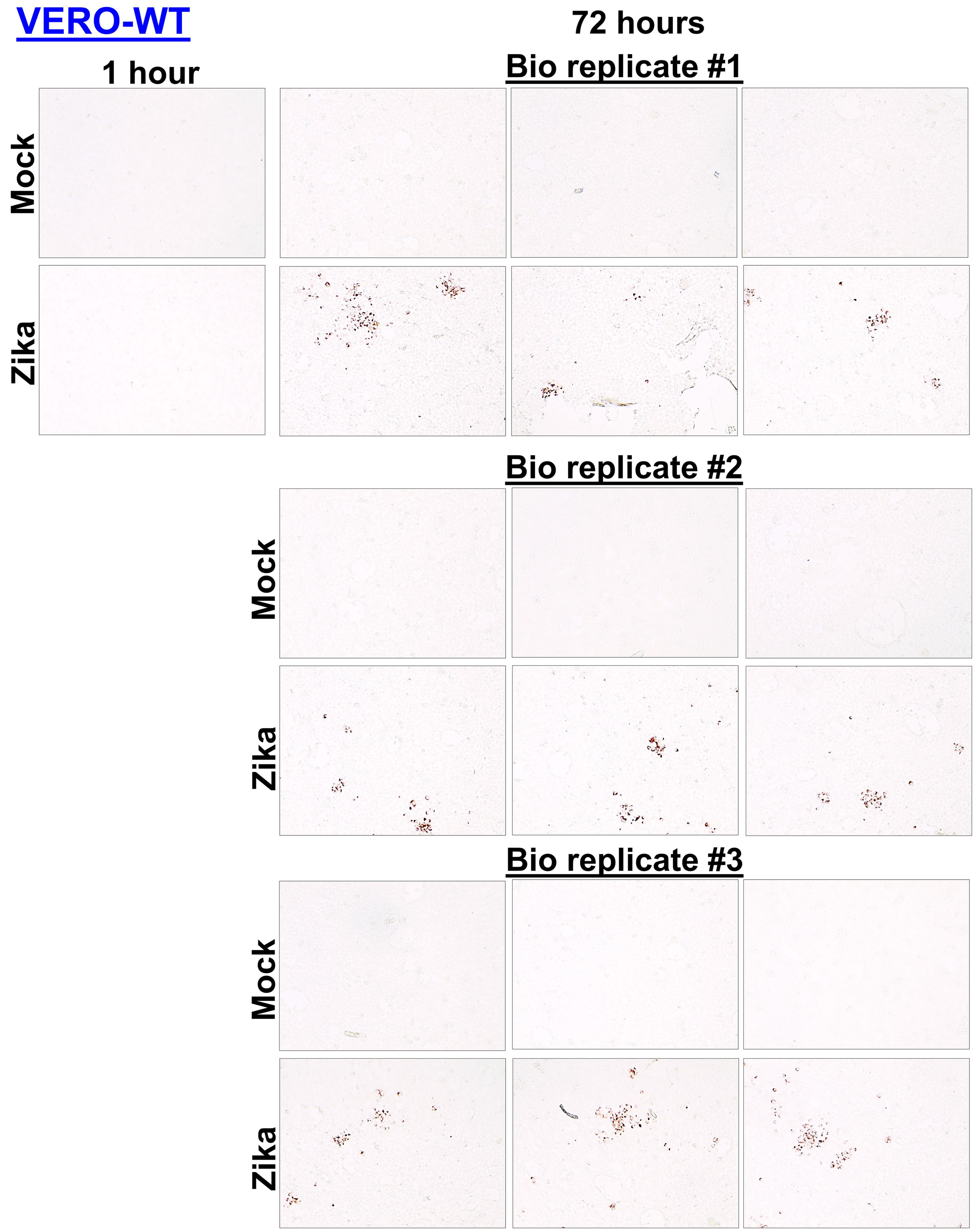
VERO-WT
1 hour
72 hours
Bio replicate #1
Mock
Zika
Bio replicate #2
Mock
Zika
Bio replicate #3
Mock
Zika

S1FigC

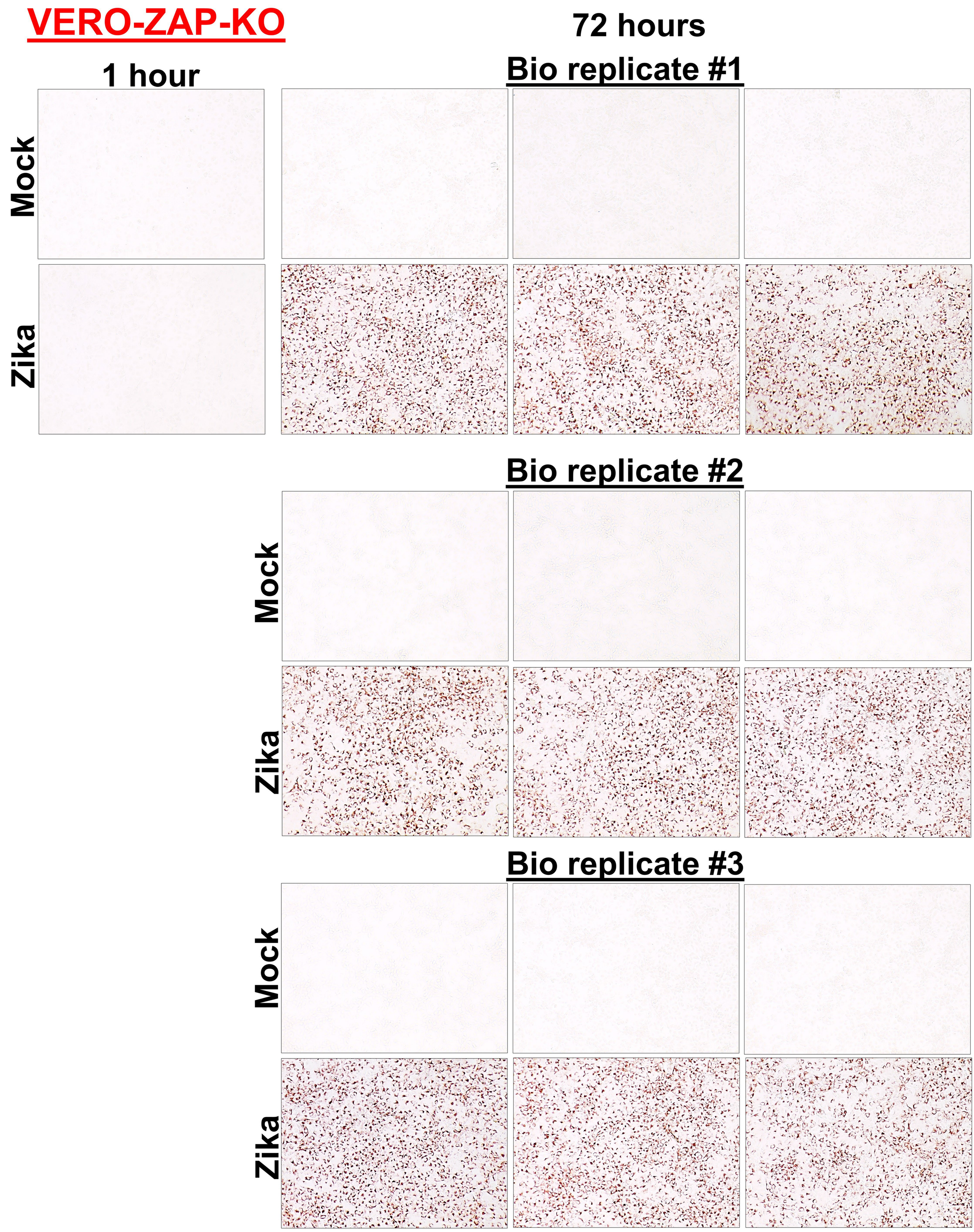
VERO-ZAP-KO
1 hour
72 hours
Bio replicate #1
Mock
Zika
Bio replicate #2
Mock
Zika
Bio replicate #3
Mock
Zika

S1FigD

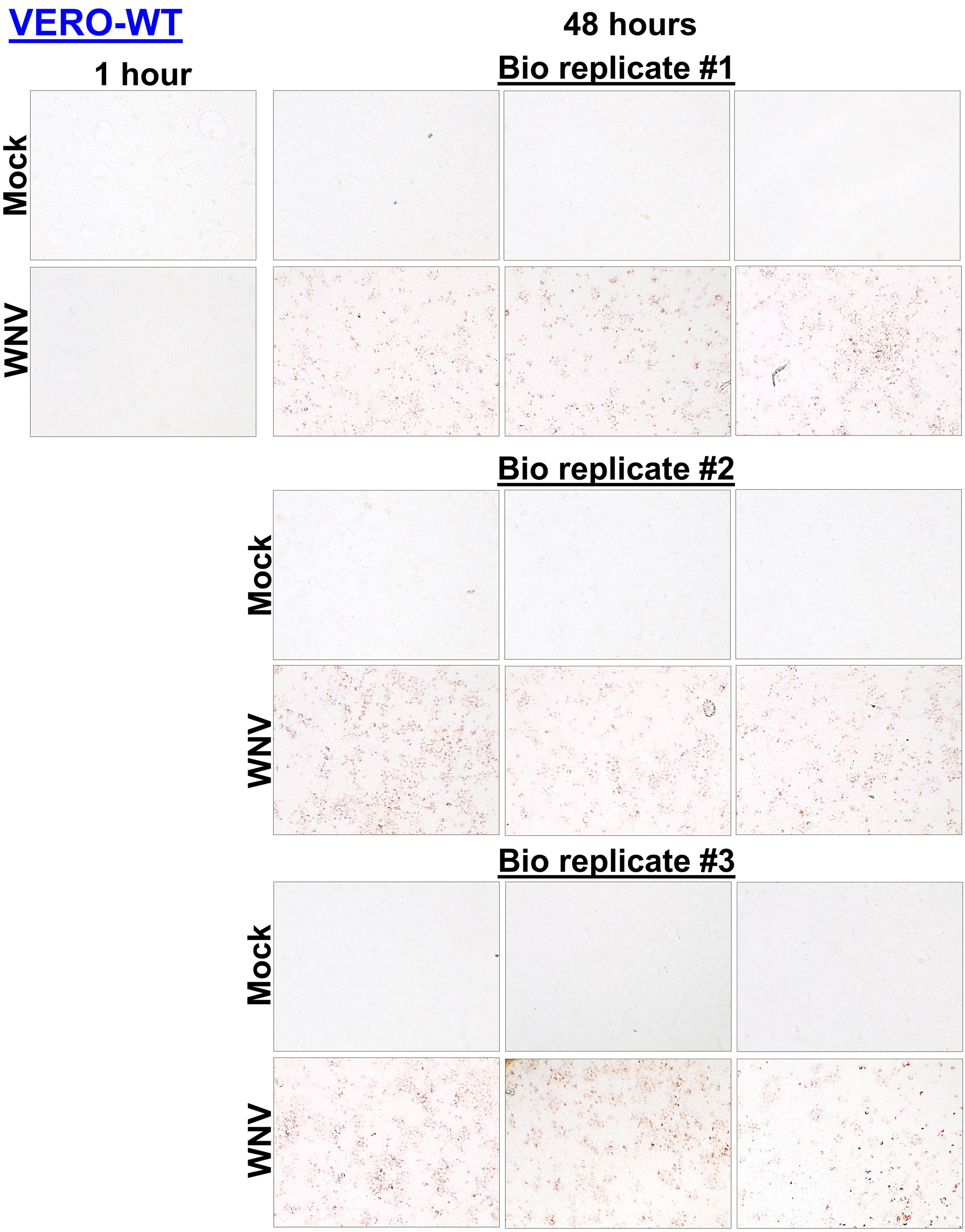
VERO-WT
1 hour
48 hours
Bio replicate #1
Mock
WNV
Bio replicate #2
Mock
WNV
Bio replicate #3
Mock
WNV

S1FigE

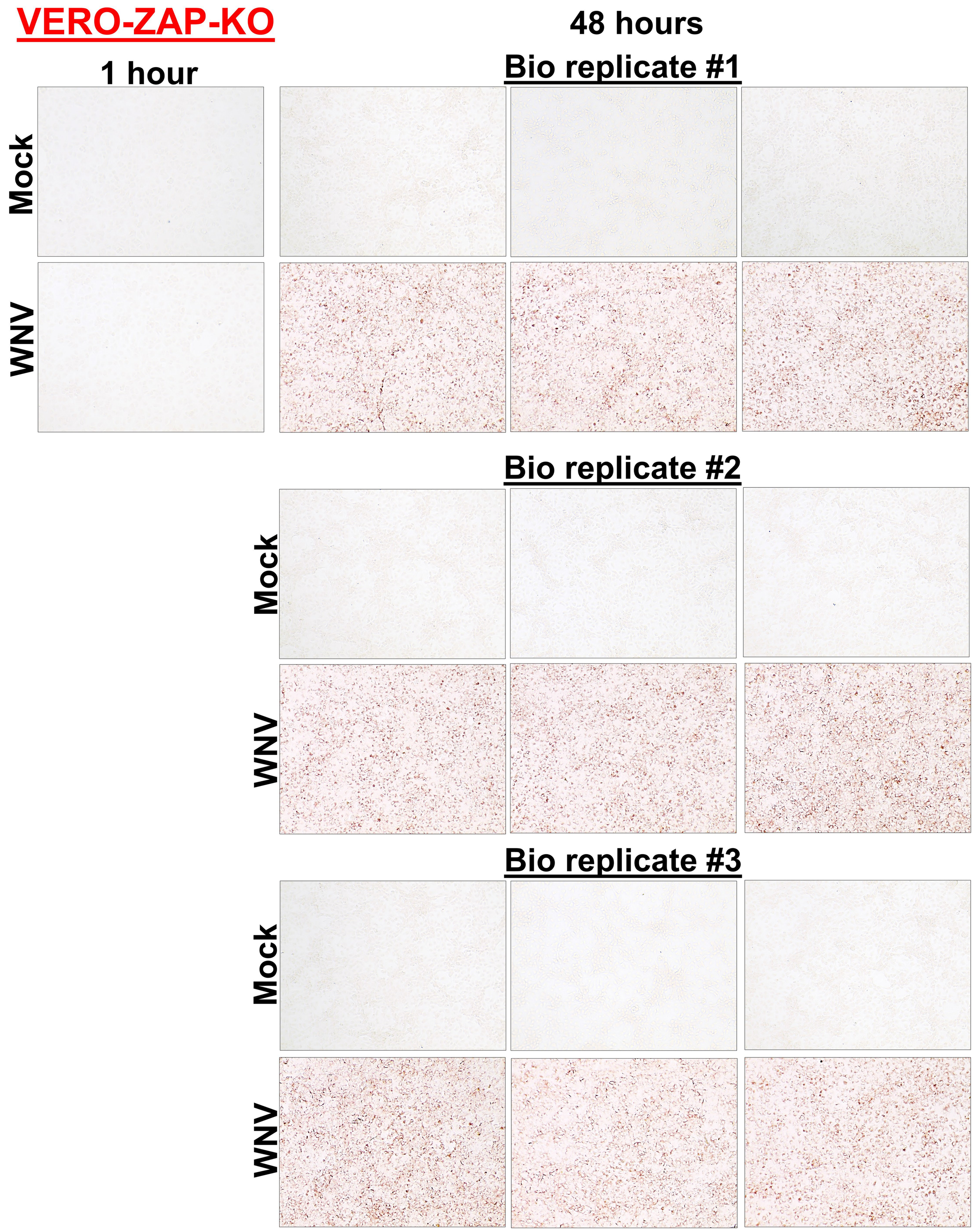
VERO-ZAP-KO
1 hour
48 hours
Bio replicate #1
Mock
WNV
Bio replicate #2
Mock
WNV
Bio replicate #3
Mock
WNV

S1FigF